

Review

Overview of Quartz Crystal Microbalance Behavior Analysis and Measurement

Sawit Na Songkhla ^{1,2,†}  and Takamichi Nakamoto ^{3,4,*,†} 

¹ Center of Excellence in Electrical Power Technology, Chulalongkorn University, Patumwan, Bangkok 10330, Thailand; sawit.n@chula.ac.th

² Department of Electrical Engineering, Faculty of Engineering, Chulalongkorn University, Patumwan, Bangkok 10330, Thailand

³ School of Engineering, Tokyo Institute of Technology, Yokohama 226-8503, Japan

⁴ Institute of Innovative Research, Tokyo Institute of Technology, Yokohama 226-8503, Japan

* Correspondence: nakamoto@nt.pi.titech.ac.jp; Tel.: +81-45-924-5017

† These authors contributed equally to this work.

Abstract: Quartz Crystal Microbalance (QCM) is one of the many acoustic transducers. It is the most popular and widely used acoustic transducer for sensor applications. It has found wide applications in chemical and biosensing fields owing to its high sensitivity, robustness, small sized-design, and ease of integration with electronic measurement systems. However, it is necessary to coat QCM with a sensing film. Without coating materials, its selectivity and sensitivity are not obtained. At present, this is not an issue, mainly due to the advancement of oscillator circuits and dedicated measurement circuits. Since a new researcher may seek to understand QCM sensors, we provide an overview of QCM from its fundamental knowledge. Then, we explain some of the recent QCM applications both in gas-phase and liquid-phase. Next, the theory of QCM is introduced by using piezoelectric stress equations and the Mason equivalent circuit, which explains how the QCM behavior is obtained. Then, the conventional equations that govern QCM behaviors in terms of resonant frequency and resistance are described. We show the behavior of QCM with a viscous film based on the acoustic wave equation and Mason equivalent circuit. Then, we present various existing QCM electronic measurement methods. Furthermore, we describe the experiment on QCM with viscous loading and its interpretation based on the Mason equivalent circuit. Lastly, we review some theoretical models to describe QCM behavior with various models.



Citation: Na Songkhla, S.; Nakamoto, T. Overview of Quartz Crystal Microbalance Behavior Analysis and Measurement. *Chemosensors* **2021**, *9*, 350. <https://doi.org/10.3390/chemosensors9120350>

Academic Editor: Boris Lakard

Received: 30 October 2021

Accepted: 5 December 2021

Published: 10 December 2021

Publisher's Note: MDPI stays neutral with regard to jurisdictional claims in published maps and institutional affiliations.



Copyright: © 2021 by the authors. Licensee MDPI, Basel, Switzerland. This article is an open access article distributed under the terms and conditions of the Creative Commons Attribution (CC BY) license (<https://creativecommons.org/licenses/by/4.0/>).

Keywords: chemical sensor; biosensor; Quartz Crystal Microbalance; vector network analyzer

1. Introduction

For more than 40 years, the Quartz Crystal Microbalance (QCM) has been one of the choices amongst many acoustic sensors due to its stability and sensitivity. The first application of quartz crystal was not a sensor but a resonator, mainly used in communications and oscillator circuits. QCM is a gravimetric sensor. Since mass is the fundamental property of an analyte, it can be monitored using acoustic devices. Its capability to detect the mass makes the acoustic resonator a universal transducer. Moreover, not only mass but other parameters are detected by QCM. It can detect very slight mass changes, around a nanogram in real-time only using a simple measurement setup. Although other acoustic devices such as a SAW (Surface Acoustic Wave) device or FBAR (Film Bulk Acoustic Resonator) can be used to detect mass, the high Q-factor characteristic of QCM enables the detection of a subtle frequency shift in comparison with those devices even if the device structure and measurement setup are simple. If the attached film is not rigid but viscous, its viscoelasticity property can also be deduced from QCM as a Q-factor. However, some measurement technique is required to extract this parameter, unlike resonant frequency, which can be estimated by the QCM oscillating frequency (if an oscillator circuit was used).

We summarize the measured parameters that are most frequently used for different types of applications in Figure 1 below.

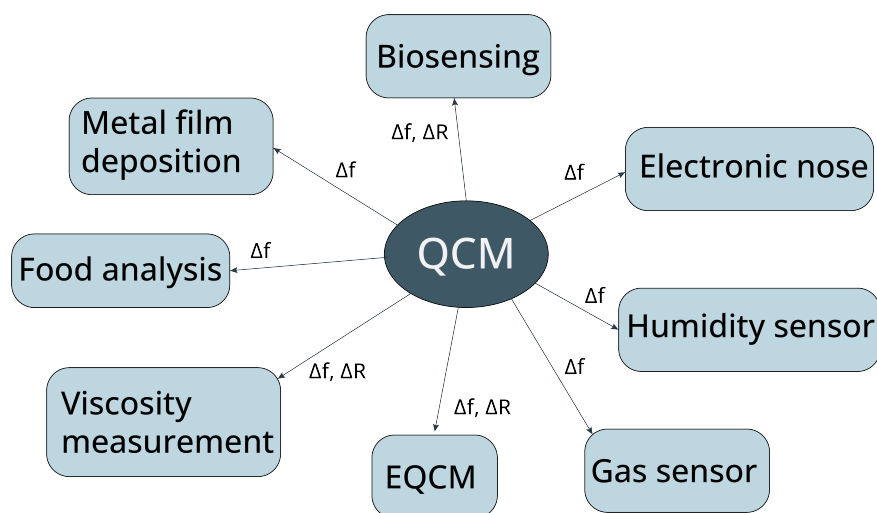


Figure 1. Measured parameters for QCM sensing applications. Δf is the QCM resonant frequency shift, and ΔR is the QCM equivalent resistance change.

QCM is a non-specific sensor and only detects the deposited mass changes. The traditional usage of a QCM sensor covers thickness monitors in metal evaporations and dissolution or corrosion [1]. Nowadays, the application expands into chemical and biosensing sensing both in the vapor phase and liquid phase. Sensing films are crucial for chemical and biosensing applications. Unfortunately, many coating materials with high selectivities and sensitivities are viscous, and viscous damping deteriorates the Q factor of QCMs.

Formerly, the QCM applications were based on an oscillator circuit where QCM is a resonator part of the circuit. Since the oscillation circuit ceases to operate due to high loss in acoustics loading, the use of viscous films or liquid-phase application becomes limited.

Nowadays, the advancements in oscillator circuit design benefit the QCM in terms of being able to operate even at a highly viscous loading [2,3]. Furthermore, some are even equipped with the function to extract the loss value or Q-factor from the QCM [4]. The classic approach to extract resonant frequency from QCM is the use of the Vector Network Analyzer (VNA). Due to its large size and high cost, it is not a suitable measurement system for on-site applications. The next approach is to use a custom-designed circuit for QCM measurement. This approach was used by many researchers, and the commercial QCM measurement system is also based on the specially designed circuit. Lastly, the development of the portable-size VNA has become ubiquitous. Many commercial products are available and have been adopted by many researchers.

As a sensor, its response should be predictable when binding between the sensor and analyte occurs. However, the QCM behavior cannot be predicted reliably by the standard models in some cases. Typically, the QCM frequency is decreased as the deposition occurs. This effect is called mass loading and was introduced by Sauerbrey in 1959 [5]. Sometimes the QCM behavior exhibits a positive frequency shift when the binding occurs [6]. This behavior cannot be explained by the mass loading effect and piques the interest of the researcher. In 1985, it was found that the QCM loaded with loose spherical particles achieved a positive frequency shift [7]. Unfortunately, biological film structure is far more complicated than a simple spherical structure. However, the concept of loosely coupling to the QCM was used to explain positive frequency change in many sensing applications [8,9].

Initially, we doubt that the positive frequency shift was due to the oscillation circuit behavior. However, it occurs even if true resonant frequency is captured. The theory based on the Mason equivalent circuit can explain it.

QCM can also be used as a label-free sensor [10–12]. The concept of label-free is the recognition of the target analyte without tagging or labeling the analyte with enzymes or fluorescent or radioactive molecules. This is based on recognizing the analyte with the binding with materials. The detection is exclusively based on its intrinsic properties, thus reducing the cost and time of the labeling step. Trending on sensor research is focused on label-free detection protocols, and QCM is one of the suitable candidate transducers for this scheme.

Although QCM has been used by many researchers, its behavior so far has not been completely understood. This paper describes the overviews of QCM behavior analysis to provide the way to accelerate the accumulation of QCM knowledge.

2. Fundamental of QCM Sensor

2.1. The Piezoelectric Effect

The QCM sensor works based on the piezoelectric effect. A certain kind of crystal under strain becomes electrically polarized. When the materials deformed, the atoms were displaced. The displacement produces electrical dipoles in the material. If the summation of these dipoles generates moments, which occurs in noninversion symmetry material, this effect is called the direct piezoelectric effect. The effect can also be reversed by applying an electrical field to the crystal, and the internal mechanical strain is generated. This reverse piezoelectric effect is the working principle of QCM.

2.2. Physical Structure

The physical structure of QCM consists of a pair of electrodes coupled with piezoelectric crystal, and typically, quartz (SiO_2) is used. If an alternating electric field with a frequency close to the resonant frequency of the crystal plate is applied to the electrode, the crystal vibrates intensely and stably (high Q factor). The simple structure of QCM is shown in Figure 2. The electrode acts an important role in energy trapping [13], which contributes to its very high Q factor, making it a very stable resonator for many electronic applications, the main oscillator, and timing circuits. Furthermore, the sensing application is the main point of this paper.

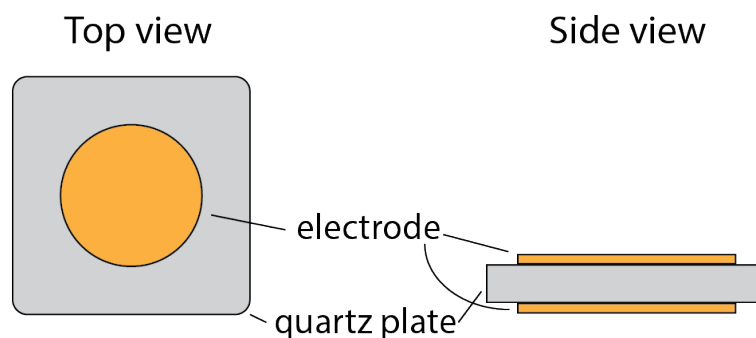


Figure 2. Basics structure of QCM.

The QCM characteristics depend on the mode of vibration and the angle at which the quartz is cut (relative to its crystallographic axes). AT-cut crystal is the most widely used, commercially available, and also used for electronic instruments. It excels in temperature stability at room temperature $25\text{ }^{\circ}\text{C}$ and operates at thickness-shear mode. This operation mode is that the displacement of the quartz is perpendicular to the quartz thickness. The crystal is cut at an angle of $35^{\circ}15'$ to the crystal z-axis. The cut provides a frequency–temperature curve with an inflection point at $25\text{ }^{\circ}\text{C}$, which means this AT cut crystal has a low-temperature coefficient around room temperature. The fundamental frequency of this crystal cut is typically between 1 and 30 MHz. QCM can also operate in overtone mode and is also widely reported for its usage [14–17]. One of the biggest advantages of QCM is its high Q factor, which can be as high as 10^6 .

2.3. Working Principle of QCM Sensor

QCM has its own natural frequency depending on the cutting angle and the thickness of the quartz crystal. The oscillation mode of QCM is called thickness-shear mode, which has the direction of displacement perpendicular to the quartz thickness with the maximum amplitude at the quartz plate surface, as shown in Figure 3.

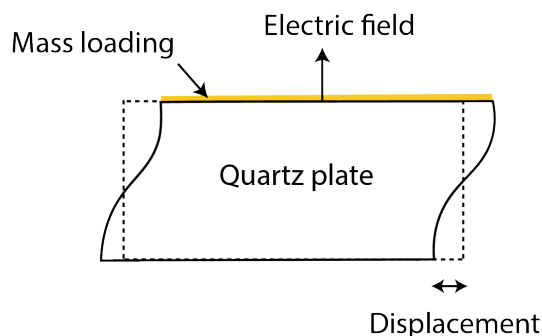


Figure 3. Thickness shear mode of Quartz Crystal Microbalance.

QCM detects the deposited mass and condition on the surface of the electrodes. For this thickness shear mode, the crystal thickness d is half of the shear mode wavelength, and we obtain

$$d = \frac{\lambda}{2}. \quad (1)$$

Let the velocity of the sound wave be v and its frequency f . Their relationship is

$$v = f\lambda. \quad (2)$$

Therefore

$$f = \frac{v}{2d}. \quad (3)$$

If the added mass acts as a thickness increase in the quartz per unit area increase by Δd , then there will be a corresponding resonant frequency change Δf as in Equation (4). This adding mass causes the reduction in resonant frequency.

$$(f + \Delta f) = \frac{v}{2(d + \Delta d)} \quad (4)$$

This is the simple explanation of the reason for the decrease in resonant frequency due to the film deposition. However, the frequency change is not governed by thickness change but mass change if the heterogeneous film is deposited. This behavior will be explained in Section 4.2.

It was found that the highest mass sensitivity of the QCM is obtained at the center, and it monotonously decreases at the location away from the center. The sensitivity curve can be approximated as a gaussian curve [18,19].

If the deposited layer over QCM is not rigid, one can expect the extra energy loss within that deposited material. This causes the Q-factor to decrease or the dissipation factor to increase. Conventional equations cover the cases of lossless film deposition and bulk liquid deposition but not the thin viscous film, which occurs in many applications. The QCM responses for various applications will be discussed in the later section.

3. Survey of QCM Study

QCM as a sensor has various applications and is so popular that there are more than 5000 publications (Listed from www.dimension.ai (accessed on 26 October 2021): Digital Science and Research Solutions, Inc., Cambridge, MA, USA) in 2020 and still growing.

However, the number of publications listed from Elsevier's Scopus database in the year 2021 is 674 publications and the trending from years 2000 to 2021 is as shown in Figure 4. This indicates its popularity as a universal chemical sensor and biosensor. The first application of QCM was mainly metal film thickness monitoring.

The QCM has been greatly adopted as biosensors in recent years, such as the improvement of QCM sensitivity using liposome anchored on a double-stranded DNA [20] or with the imprinted polymer technology for insulin detection [21]. The detection of three strains of *E. coli*. was achieved by using antibody and the surface modification of QCM by Sulfo-SMCC [22]. In this publication, they use both an oscillator circuit and network analyzer as measurement methods. The high fundamental frequency QCM (HFF-QCM) immunosensor with a frequency of 100 MHz was developed for the detection of pesticide carbaryl and thiabendazole [23]. The data were compared with standard and optimized ELISA (Enzyme-Linked Immuno Sorbent Assay), SPR (Surface Plasmon Resonance) and various low-frequency QCM sensors. They reported that 100 MHz HFF-QCM has higher sensitivity and better performance than SPR and QCMs with lower fundamental frequencies, and it achieved comparable performance as the standard ELISA method.

EQCM (Electrochemical Quartz Crystal Microbalance) is the technique that combines an electrochemical cell and a QCM sensor. This opens the possibility of detecting the mass deposition together with the ability to control and monitor the reactions and, at the electrode surface, using potentiostat. It was dated back as far as 1985 by Schumacher et al., who monitored the oxidation of a gold electrode and found that the surface roughness causes additional mass loading due to the trapped liquid [24]. Research in recent years also revolved around the study of the reaction of adsorption and deposition of battery mechanisms by using EIS (Electrochemical Impedance Spectroscopy) and EQCM to create a system for studying both physical and chemical changes [25]. This system employed the commercial QCM-D system, which can measure both resonant frequency and dissipation. This makes it possible to estimate film mass, film viscosity, film modulus and electrolyte viscosity from their model.

Furthermore, the applications of QCM in liquid viscosity measurements are still popular, such as a sensor that operates in harsh environments such as extreme temperature, acidity and pressure. B. Acharya et al. show the study of QCM in measuring high viscous oils at high temperatures [26]. Their apparatus consists of a stainless steel QCM chamber, and their temperatures range from 25 to 200 °C. Their result shows good fitting with conventional equations with a correction factor based on the QCM surface roughness effect. The application of liquid viscosity measurement in a lead-acid battery was also reported [27]. The QCM sensor also has been used for detecting the flow assurance problem in the petroleum industry [28].

Lastly, many commercially available measurement systems make it easier for researchers to use QCM without the need to create a measurement system. Table 1 is a selection of publications on QCM sensing from recent years.

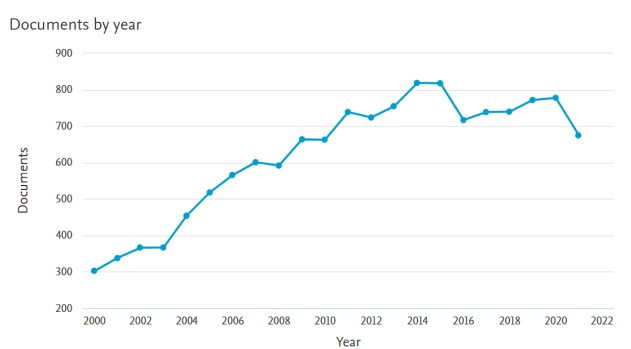


Figure 4. Trends of the QCM publications.

Table 1. Selection of the recent QCM studies.

Title	Application	Coating Material	Analyte	Features	Ref.
Fabrication of highly sensitive QCM sensor using anodic aluminum oxide (AAO) nanoholes and its application in biosensing	Biosensing	mouse IgG	anti-mouse IgG	Increased QCM sensor sensitivity with the AAO nano well structure on the measuring an antigen-antibody interaction	[29]
Acoustic methodology for selecting highly dissipative probes for ultrasensitive DNA detection	Biosensing	Liposome/ DNA complex	DNA	Liposomes anchored to a dsDNA chain led to an improvement of the limit of detection (LoD) by 3 orders of magnitude when compared to direct DNA detection	[20]
Target-triggering multiple-cycle signal amplification strategy for ultrasensitive detection of DNA based on QCM and SPR	Biosensing	Streptavidin-coated AuNPs (gold nanoparticles)	DNA	A signal amplification process, including the exonuclease III and the hybridization chain reaction (HCR) of DNA. The reaction was detected by a QCM sensor together with SPR sensor. It exhibited a high sensitivity toward target DNA with a detection limit of 0.70 fM	[30]
Classification of multiple Chinese Liquors by Means of a QCM-based E-Nose and MDS-SVM Classifier	Electronic nose	PVC, Polyamide, Polyethlyene, Polytef, AgCl, Azithromycin, CuCl ₂	Various Chinese liquors	Identify the different types of Chinese liquors using an array of QCM with an SVM classifier. The prediction accuracy (98.3%) showed superior performance of the MDS-SVM classifier over the back-propagation artificial neural network (BP-ANN) classifier (93.3%) and moving average-linear discriminant analysis (MA-LDA) classifier (87.6%)	[31]
An investigation about the origin of the lung cancer signaling VOCs in breath	Electronic nose	RuTPP, RhTPP, MnTPP, CoTPP, SnTPP, CoNO ₂ TPP, CoOCH ₃ TPP, MnOMC	Exhale breath sample from cancer patients	Partial Least Squares Discriminant Analysis (PLS-DA) has been used. The electronic nose could discriminate between cancer and non-cancer patients with more than 90% correct classification	[32]

Table 1. Cont.

Title	Application	Coating Material	Analyte	Features	Ref.
Electronic nose system based on Quartz Crystal Microbalance sensor for blood glucose and hba1c levels from exhaled breath odor	Electronic nose	Zeolites, fullerene C60, chiral materials, polypyrrole, carbon graphites, ITO films, oligonucleotides	Exhale breath sample	The study of exhale gas to detect Blood Glucose and HbA1c level using a radial basis function neural network (RBFNN). The accuracies were 83.03% and 74.76% for HbA1c parameter predictions and glucose parameter prediction	[33]
An ultrasensitive electrochemical impedance-based biosensor using insect odorant receptors to detect odorants	Electronic nose	Odorant receptors (ORs): Or10a, Or22a, Or35a, Or71a	Methyl salicylate, E2-hexenal, 4-ethylguaiaicol	OrX/Orco liposomes could sensitively and selectively detect their ligands by monitoring a change in frequency and dissipation signal of Quartz Crystal Microbalance	[34]
Application of Quartz Crystal Microbalance with dissipation (QCM-D) to study low-temperature adsorption and fouling of milk fractions on stainless steel	Food analysis	Stainless steel(SS2343)	Whole milk, skim milk, acid whey, acid permeate	acid whey (pH 4.6) demonstrated significant constant-rate adsorption at long processing times. It is anticipated that linear adsorption rates at extended times can be used to predict fouling propensity at a commercial scale	[35]
Novel Quartz Crystal Microbalance immunodetection of aflatoxin B ₁ coupling cargo-encapsulated liposome with indicator-triggered displacement assay	Food analysis	Glucose-loaded nanoliposome, labeled with monoclonal anti-AFB1 antibody	Aflatoxin B ₁	QCM response showed a good linear relationship between the frequency shift, and AFB1 concentration could be obtained within the dynamic working range from 1.0 ng kg ⁻¹ to 10 mg kg ⁻¹	[36]
Fabrication of a Quartz Crystal Microbalance sensor based on graphene oxide/TiO ₂ composite for the detection of chemical vapors at room temperature	Gas sensing	Graphene oxide (GO)/TiO ₂	Ethanol vapor	The sensitivity of the composite functionalized QCM resonator for the EtOH vapor ranged from 8300 to 20 ppm	[37]
Highly sensitive and chemically stable NH ₃ sensors based on an organic acid-sensitized cross-linked hydrogel for exhaled breath analysis	Gas sensing	Acid-sensitized cross-linked poly(ethylene glycol) diacrylate (PEGDA) hydrogel	NH ₃	CA (Citric Acid)/PEGDA and MA(Malic Acid)/PEGDA sensors exhibit a response as low as 0.05 ppm NH ₃	[38]
Humidity Sensing Properties of Metal Organic Framework-Derived Hollow Ball-Like TiO ₂ Coated QCM Sensor	Humidity sensor	TiO ₂ Nanopowder	Humidity	The sensor indicates a large frequency change with an interaction that occurred between TiO ₂ and humidity molecules. The sensor exhibited a good repeatability when it was exposed to the moist air of 65% RH	[39]

Table 1. Cont.

Title	Application	Coating Material	Analyte	Features	Ref.
Quartz crystal microbalance apparatus for the study of viscous liquids at high temperatures	Viscosity measurement	N/A	Liquid viscosity	The study of QCM in measuring high viscous oils at high-temperature range from 25 to 200 °C	[26]
Resolution in QCM Sensors for the Viscosity and Density of Liquids: Application to Lead Acid Batteries	Viscosity measurement	N/A	Liquid viscosity	The application of liquid viscosity measurement in lead-acid battery. The findings show that the resolution limit only depends on the characteristics of the liquid to be studied and not on frequency	[27]
Operando EQCM-D with Simultaneous in situ EIS: New Insights into Interphase Formation in Li-Ion Batteries	EQCM	Super C65 Carbon, lithium iron phosphate (LiFePO ₄)	N/A	QCM with dissipation monitoring (EQCM-D) with simultaneous in situ electrochemical impedance spectroscopy (EIS) has been developed and applied to study the solid electrolyte interphase (SEI) formation on copper current collectors in Li-ion batteries	[25]
QCM sensing of bisphenol A using molecularly imprinted hydrogel/conducting polymer matrix	EQCM	Cyclodextrin-modified poly(L-lysine) (CD-PLL)	Bisphenol A (BPA)	The BPA-imprinted CD-PLL gel layer chip showed a greater Δf in response to BPA than the non-imprinted CD-PLL gel layer chip and the directly CD-immobilized chip	[40]

4. Theory of QCM

To be able to utilize QCM effectively, understanding QCM behavior in the common environment is necessary. Furthermore, studying the mathematical model helps researchers understand the underlying physical phenomenon and improve the interpretation. In this section, starting with the equivalent circuit derived from the acoustic wave propagation equation with the Mason equivalent circuit, we analyze its behavior with different boundary conditions for different QCM loading effects.

4.1. Equivalent Circuit

One approach to represent the acoustic properties of the QCM with various coatings is to use a one-dimensional solution of piezoelectric stress equations. This is shown with the assumption of an infinite quartz plate area (lateral axis) in Figure 5 [41]. The acoustic impedance, which is derived from piezoelectric stress equations, describes the acoustic load concept of QCM. The Mason equivalent circuit is shown in Figure 6, which represents the behavior of acoustic loading at both electrode surfaces (PORT1 and PORT2) and translates them as electrical impedance at the electrical port (PORT3) [42]. The model identical to this one may be called a transmission line, as in some other publications [43,44]. Z_0 is the characteristic acoustic impedance multiplied by the surface area S_A . ϕ is the transformer ratio. Z_1 and Z_2 are purely reactive.

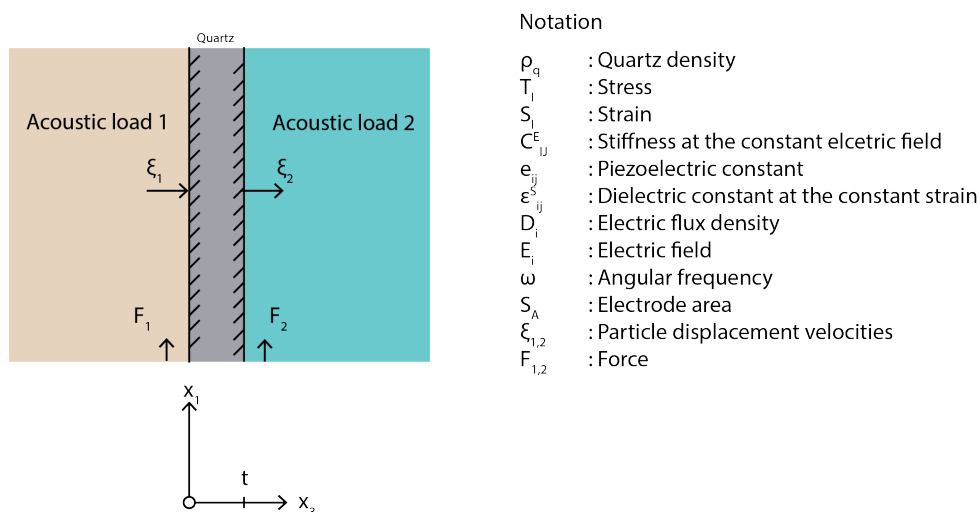


Figure 5. Coordinate system and notation used in this analysis.

$$Z_1 = jZ_0 \tan(\omega l / 2v_q), \quad Z_0 = \rho_q v_q S_A$$

$$Z_2 = -jZ_0 / \sin(\omega l / v_q), \quad \Phi = e_{35} \cdot S_A / t$$

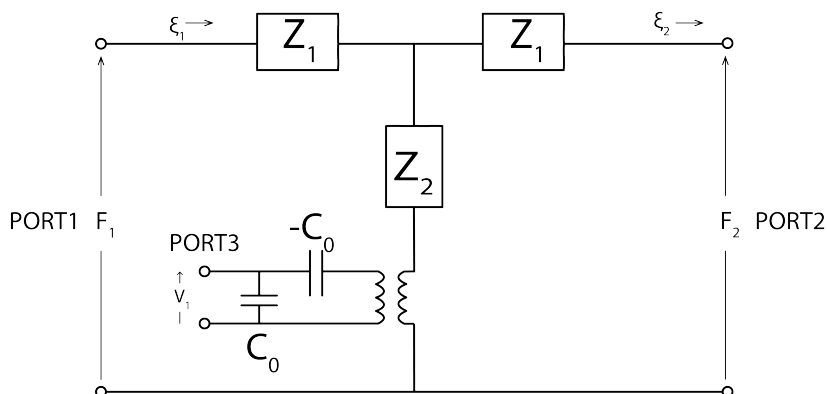


Figure 6. Mason equivalent circuit.

The mason equivalent circuit can be further simplified, which is beneficial to the interpretation of the QCM response. Typically, one surface of the QCM is unloaded, shorting the circuit on the left-hand side. The acoustic load Z_3 is connected to PORT2. Z_4 is the impedance seen from the dashed line to the right side. It is given by

$$Z_4 = Z_2 + \frac{Z_1(Z_1 + Z_3)}{2Z_1 + Z_3}. \tag{5}$$

The further simplified Mason circuit is shown in Figure 7. Since Z_1 and Z_2 were defined in terms of Z_0 , we rearranged the Z_1, Z_2 and Z_3 into Z_5, Z_6 and Z_7 . The Equation (5) is changed to

$$Z_4 = Z_5 + \frac{1}{1/Z_6 + 1/Z_7} \tag{6}$$

where:

$$Z_5 = (-j/2)Z_0 \cot \frac{\omega t}{2v_q}, \tag{7}$$

$$Z_6 = \frac{Z_3}{4} \tag{8}$$

and

$$Z_7 = j\frac{Z_0}{2} \tan \frac{\omega t}{2v_q}. \tag{9}$$

Utilizing Mittag-Leffer’s theorem, the tangent function can be expanded as

$$\frac{\tan a}{a} = \sum_{n \text{ odd}} \frac{P_n}{1 - (a/a_n)^2}. \tag{10}$$

where

$$P_n = \frac{1}{n^2} \frac{8}{\pi^2}, a_n = n\pi/2. \tag{11}$$

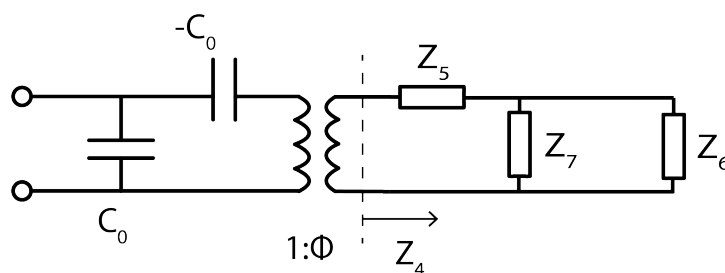


Figure 7. Modified Mason equivalent circuit.

Z_5 is composed of several series of LC circuits connected in parallel, where each one represents harmonic resonance frequencies, as shown in Figure 8 [45]. Z_5 can be expressed as

$$Z_5 = \frac{1}{1/(-j(Z_0/2P_1a) + j(1/2)Z_0(a/P_1a_1^2))} + 1/(-j(Z_0/2P_3a) + j(1/2)Z_0(a/P_3a_3^2)) + \dots = 1/ \sum_{n \text{ odd}} (1/ - j(\omega C_{sn}) + j\omega L_{sn},) \tag{12}$$

where $a = \omega/2v_q, L_{sn}$ and C_{sn} for the n th harmonic are

$$L_{sn} = \frac{\rho_q t^3}{8e_{35}^2 S_A} \tag{13}$$

and

$$C_{sn} = \frac{1}{n^2} \frac{8}{\pi^2} \frac{S_A}{C_{55}^D} \frac{e_{35}^2}{t}, \text{ respectively.} \tag{14}$$

Similarly, the Z_7 can also be expanded as

$$Z_7 = j \frac{Z_0}{2} \tan \frac{\omega t}{2v_q} = \sum_{n \text{ odd}}^{\infty} \frac{1}{(1/j\omega L_{pn}) + j\omega C_{pn}} \tag{15}$$

where $L_{pn} = (1/n^2)L_{p1}$, $L_{p1} = \rho_q S_A t (2/\pi^2)$ and $C_{pn} = C_{p1} = 2t/S_A C_{55}^D$ (C_{55}^D is the stiffness at the constant dielectric flux density). However, Z_7 can be eliminated since it becomes infinite around $\omega = nv_q/2t$. Then the circuit is reduced to Figure 8 when the transformer in Figure 7 was further simplified. If the harmonics are not considered, the circuit is simplified to the Butterworth–Van Dyke (BVD) circuit, as shown in Figure 9.

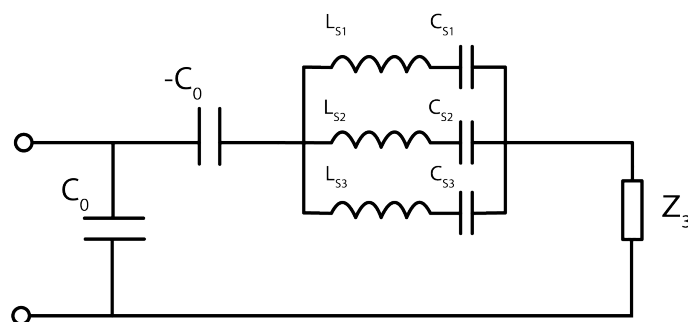


Figure 8. Simplified equivalent circuit for harmonics.

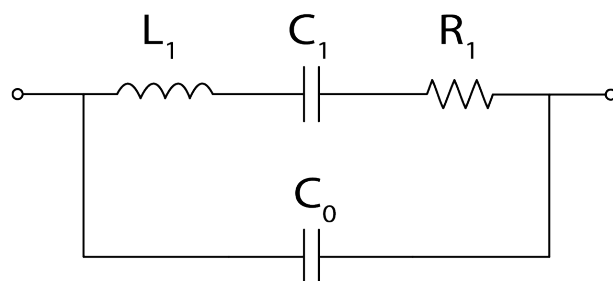


Figure 9. Butterworth–Van Dyke model.

The BVD circuit can simply explain QCM behavior near the resonant frequency. The motional admittance plot of the BVD circuit is shown in Figure 10. The arrows indicate the direction of frequency sweep near the QCM resonant frequency.

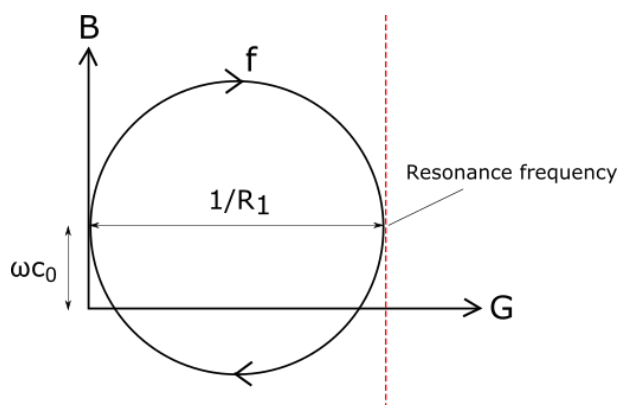


Figure 10. Admittance plot of QCM.

The admittance plot is a circle with the Y-offset equal to ωC_0 if ωC_0 is considered constant around the resonant frequency value. The series resonance frequency is the right-most point of the admittance plot, which has the maximum conductance value. The distance from the y-axis to this point is the reciprocal of the resistance R_1 in the BVD equivalent circuit.

The admittance of the BVD circuit is expressed as

$$Y = \frac{1}{R_1 + j\omega L_1 - \frac{1}{j\omega C_1}} + j\omega C_0. \quad (16)$$

Considering only the real part of admittance (conductance), the equation can be rearranged as

$$G = \frac{R_1}{R_1^2 + \left(2\pi f L_1 - \frac{1}{2\pi f C_1}\right)^2}. \quad (17)$$

Equation (17) includes only circuit components from the resonant part without involving C_0 . This is useful for extracting the resonant frequency and the resistance value using only conductance.

4.2. QCM Behavior

The usage of QCM as a sensor can be applied to both gas and liquid phases. Commonly, the frequency of oscillation is measured. The interaction of the analyte to the sensing film on the electrode causes the frequency to change. This frequency change is translated to the inductance change in the BVD circuit. Firstly, the application of QCM was limited to the gas phase because, in the liquid phase, the viscosity impedes the oscillation of the QCM and its inability to maintain the positive oscillation feedback made it stop operating. This drawback does not persist in the current day. The development of a more stable oscillator circuit, the design of a dedicated circuit for QCM measurement, and the use of the Vector Network Analyzer enables us to measure the resonance frequency even under the situation of the deterioration of quality factor. Numerous applications of chemical and biological sensors are feasible in both gas and liquid phases. The Mason equivalent circuit can represent these behaviors by providing appropriate boundary conditions.

4.2.1. Gas Phase

The decrease in frequency due to mass deposition was first explained by Sauerbrey as follows.

$$\Delta f = - \frac{2f_0^2}{S_A \sqrt{\rho_q \mu_q}} \Delta m, \quad (18)$$

where:

f_0 —Resonant frequency of the fundamental mode (Hz)

Δf —Frequency change (Hz)

Δm —Mass change (g)

S_A —Electrode area (cm²)

ρ_q —Density of quartz (g/cm³)

μ_q —Shear modulus of quartz for AT-cut crystal (g cm⁻¹ s⁻²)

Equation (18) can be derived from the previous impedance analysis [41].

Sauerbrey explicitly describes the response to mass change. However, it does not consider the viscosity of the solution if the QCM is used in a liquid environment. Furthermore, its interpretation is limited to only rigid, thin-film and has to be firmly attached to the QCM electrode.

Sauerbrey's equation is applicable for measuring small amounts of deposition and can be used to monitor coating film thickness since, at the small film thickness, the effect of loss due to viscosity is less significant than the amount of deposited mass, which is the film thickness itself, and approximately 2% of deposited mass has good agreement with

Sauerbrey's equation. The large mass loading was also investigated. Lu and Lewis used the vacuum deposition of various metals over QCM with a gold electrode and found that the deviation from Sauerbrey's equation occurs at high mass loading (more than 15% of the quartz plate mass). Their derived one-dimensional acoustic composite-resonator model works even in the case of large mass loading [46].

A further investigation of the localized response of QCM to the loss was conducted and found that the sensitivity distribution of QCM follows the shape of the Gaussian curve using an empirical formula [47]. The experiment was thoroughly investigated by localized mass deposits created by electrochemical deposition. The highest sensitivity of the QCM is at the center of the electrode, then it decreases monotonously and extends slightly beyond the electrode edge [18].

4.2.2. Liquid Phase

The application of QCM in liquid is dated back to 1985 by Kanazawa [48]. His calculation was based on a shear wave velocity of liquid in contact with the quartz plate. His equation is defined as

$$\Delta f = -f_0^{3/2} \left(\frac{\eta_l \rho_l}{\pi \rho_q \mu_q} \right)^{1/2}. \quad (19)$$

where:

f_0 —Resonant frequency of the fundamental mode (Hz)

η_l —Liquid viscosity (cP)

ρ_l —Liquid density (g/cm³)

ρ_q —Density of quartz (g/cm³)

μ_q —Shear modulus of quartz for AT-cut crystal (g cm⁻¹ s⁻²)

Equation (19) can be derived from the previous impedance analysis [41].

This equation is based on vanishing shear wave into liquid. The distance the wave can travel into liquid is called viscous penetration depth (Figure 11), as is given in Equation (20). The shear wave amplitude drastically attenuates at the point away from the quartz plate.

$$\lambda = \frac{1}{2} \left(\sqrt{\frac{\rho_L \omega}{2\eta}} \right)^{-1} \quad (20)$$

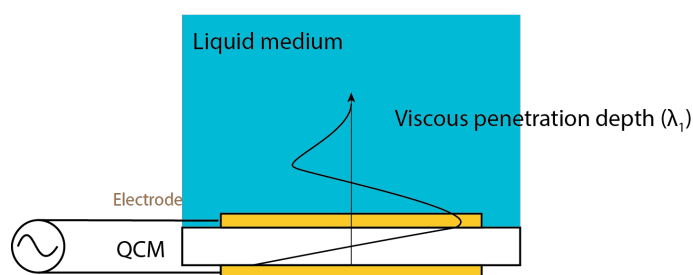


Figure 11. Penetration of QCM immersed in liquid medium.

The concept of viscous penetration depth should define the maximum thickness of the liquid layer over the QCM that still influences the frequency shift. The frequency change is caused by the viscosity or density change of the liquid layer.

However, many researchers found that the QCM responses are much more complicated. Sometimes the QCM frequency shifts even if the perturbation is beyond the penetration depth. Furthermore, the unusual case was a positive frequency shift when exposed to the measure, and Kanazawa's equation is too simplified and did not consider coating layer thickness, which is one of the important parameters for sensor response when a liquid layer instead of bulk liquid is coated over QCM, which sometimes occurs in the experiment. Furthermore, similar to Sauerbrey's equation, the positive frequency change cannot be explained by Kanazawa's equation.

4.3. Film Behavior

Generally, to use QCM as sensors, coating materials are required to let QCM have specificity and sensitivity. This scheme differs from mass sensing and bulk liquid sensing. A more complicated response from QCM can occur. The boundary condition of rigid film into the viscous film is extended by replacing the shear wave velocity term of a rigid film with shear wave velocity in liquid. The analysis based on the Mason equivalent circuit is still adequate in predicting a viscous film response.

Let us define Z_{eL} as the loading from the deposited viscous film. This loading added extra impedance to the resonant circuit of the BVD circuit, as is shown in Figure 12.

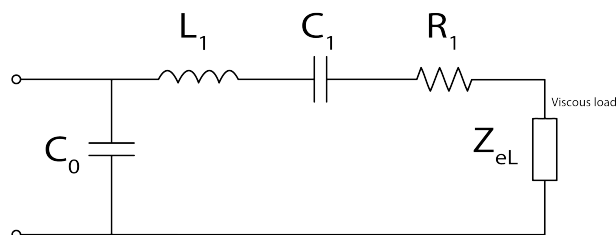


Figure 12. The equivalent circuit of the Quartz Crystal Microbalance (QCM), the Butterworth–Van Dyke model with viscous loading.

Figure 13 shows the coordinate system of QCM coated with thin film. This model is the case of viscous thin-film, where ω is the angular frequency, μ is shear modulus and v_{A1} is the complex shear wave velocity. The particle displacement u_1 and the shear stress T_5 are given by

$$u_1 = Ae^{-j(\omega/v_{A1})x_3} + Be^{j(\omega/v_{A1})x_3} \tag{21}$$

and

$$T_5 = \mu S_5 = \mu \frac{\partial u_1}{\partial x_3} = j \frac{\omega}{v_{A1}} \mu \left(-Ae^{-j(\omega/v_{A1})x_3} + Be^{j(\omega/v_{A1})x_3} \right), \tag{22}$$

where A and B are constant. At the film surface ($x_3 = t + h$), the stress is considered free ($T_5 = 0$). The ratio of A to B can be solved to

$$\frac{A}{B} = e^{j(2\omega/v_{A1})(t+h)}. \tag{23}$$

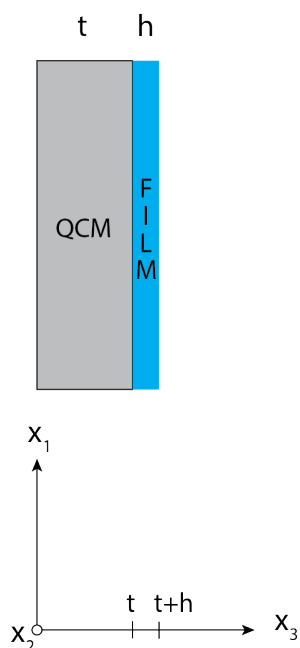


Figure 13. Model of viscous film.

Using Equations (21)–(23), the piezoelectric stress equation can be solved to obtain the acoustic impedance Z_L

$$Z_L = -\frac{T_5}{j\omega u_1} \Big|_{x_3=t} = \frac{\mu}{v_{A1}} \frac{1 - e^{j(2\omega/v_{A1})}}{1 + e^{j(2\omega/v_{A1})}} = j\rho_L v_{A1} \tan \frac{\omega h}{v_{A1}} \tag{24}$$

where ρ_L is film density and h is film thickness. The shear wave of viscous film was calculated differently by replacing the strain velocity with the stress equation. We obtain

$$\rho_L \frac{\partial^2 u_1}{\partial t^2} = \frac{\partial T_5}{\partial x_3} \tag{25}$$

and

$$T_5 = j\omega\eta_L S_5, \tag{26}$$

where η_L is liquid film viscosity. Substitute Equation (26) into (25), and the wave velocity is

$$v_W = \sqrt{\frac{j\omega\eta_L}{\rho_L}}. \tag{27}$$

Replacing v_{A1} in Equation (24) with v_W we obtain

$$Z_L = j\sqrt{j\rho_L\eta_L}\omega \tan(\omega h \sqrt{\frac{\rho_L}{j\omega\eta_L}}). \tag{28}$$

Electrical impedance Z_{eL} is expressed as

$$Z_{eL} = \frac{t^2 Z_L}{4e_{35}^2 S_A} = \frac{t^2}{4e_{35}^2 S_A} j\sqrt{j\rho_L\eta_L}\omega \tan(\omega h \sqrt{\frac{\rho_L}{j\omega\eta_L}}) \tag{29}$$

where t is quartz thickness, e_{35} is the piezoelectric constant and S_A is the QCM electrode area.

The simulation using this Equation (29) with the values of the parameters of water as film material is shown in Figure 14. The frequency change is calculated from the change of resonant frequency, which is calculated from the equation $\Delta f = \frac{1}{2\pi\sqrt{(L_1+\Delta L_1)C_1}} - f_0$ where $\Delta L_1 = \frac{\text{imag}(Z_{eL})}{2\pi f_0}$, and f_0 is the resonant frequency, calculated from $f_0 = \frac{1}{2\pi\sqrt{L_1C_1}}$.

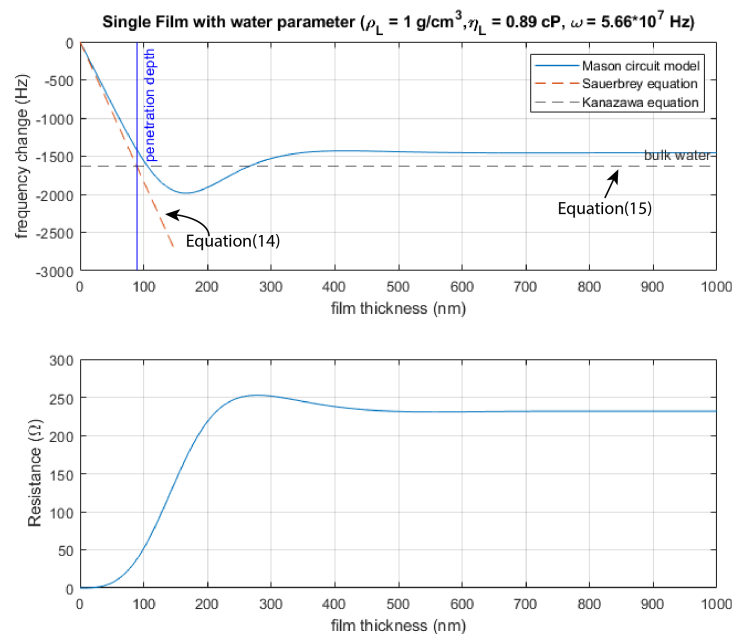


Figure 14. QCM response simulation using Mason equivalent circuit and parameters of water.

The simulation using water parameters of 9 MHz QCM and water, $\rho_L = 1 \text{ g/cm}^3$, $\eta_L = 0.89 \text{ cP}$, $\omega = 5.66 \times 10^7 \text{ Hz}$, $S_A = 0.196 \text{ cm}^2$, $e_{35} = -0.095$, $L = 12.65 \text{ mH}$, $C = 2.47 \times 10^{-14} \text{ F}$. The variable here is film thickness (h). The simulation showed that the frequency change at small loading agrees with Sauerbrey's equation and at infinite film thickness, the frequency change converges to that of Kanazawa's equation. When the film thickness becomes larger than the viscous penetration depth, it exhibits an interesting transition. Consider the frequency change of the figure. The negative frequency continues to decrease as the film thickness increases until about 170 nm. Then, the direction of frequency shift inverses toward increasing and then saturates. The resistance change follows a similar trend, but the resistance increases first and until around 260 nm slightly decreases and then saturates. Interestingly, the turning points of the frequency shift and resistance are different film thicknesses. This property becomes important in explaining why positive frequency change occurs while the resistance still increases.

Figure 15 shows the simulation while varying the viscosity from 1 to 10 cP, assuming that liquid density is constant. The plot shows that the film thickness with the minimum frequency change increases as the viscosity increases. The overall negative frequency change also increases.

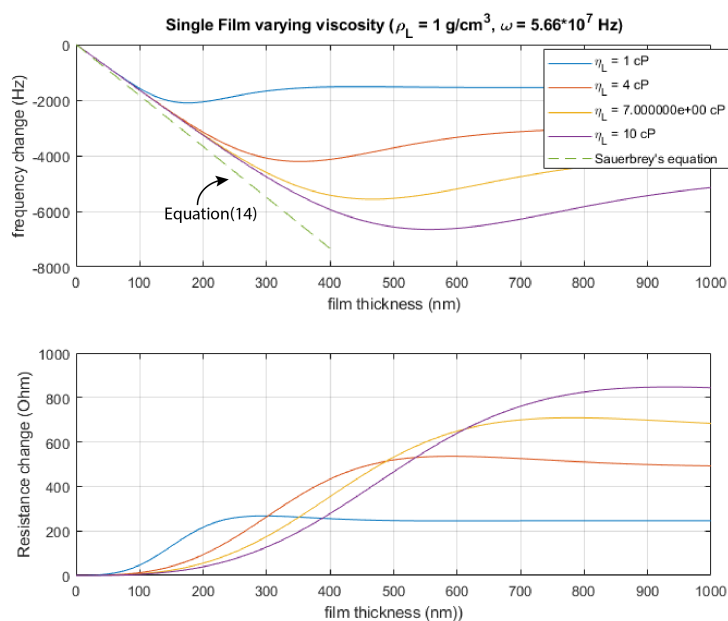


Figure 15. QCM response simulation using Mason equivalent circuit varying viscosity.

Equation (24) can explain both rigid film and liquid loading. Thus, it provides a general analysis method of QCM behavior. We summarize the general guidelines for applying the equations in Table 2.

Table 2. General application guideline of QCM behavior equations.

QCM Applications	Equations	Limitation
Thin film	Sauerbrey's equation (Equation (18))	For rigid film, it can be applied to several micrometers of film thickness. It is still applicable to viscous film if the film thickness is substantially less than the viscous penetration depth of that viscosity.
Bulk liquid	Kanazawa's equation (Equation (19))	Only applicable to non-newtonian bulk liquid.
Viscous film	Mason equivalent with the viscous film boundary condition (Equation (29))	It can be applied to viscous film with its arbitrary thickness.

5. QCM Measurement Methods

The quartz crystal oscillator used in microcomputers was developed by W. G Cady in 1922 [49]. The first QCM oscillator consists of a three-staged amplifier with a feedback loop. With this similar structure, QCM can also be operated as an oscillator and measure the mass loading effect by indirectly estimating from oscillation frequency instead of the resonant frequency. However, as the damping becomes larger, the lower Q factor is challenging in terms of maintaining a stable oscillation. To tackle this issue, a significant amount of research on the QCM measurement method was conducted, including the improvement of the oscillator circuit design or the development of a dedicated circuit to extract the QCM resonant frequency. Lastly, the research highlights a compact-size Vector Network Analyzer, which has become more available at lower costs in recent years. We will discuss several of these QCM measurement methods in detail in the next section.

5.1. Oscillator Circuit

The most basic circuit incorporating QCM is the pierce oscillator (Figure 16). The circuit consists of a digital inverter, a feedback resistor, and two capacitors. This design is used throughout microcomputer technology due to its simple design and good stability of clock generating application. The application of the Pierce oscillator under full liquid immersion was investigated [50]. However, many design considerations need to be made and it does not work well under heavy viscous loading. There is the proposal of double-resonance using the Pierce oscillator topology by Satoh et al. [51]. Their design works in both single-sided or complete water immersion. The oscillation frequency is controlled by a variable capacitor, which can be adjusted to lock the oscillation frequency to the desired operating condition. The design with a variable-capacitance diode to improve its capability in the ease of controlling oscillation frequency was reported [52].

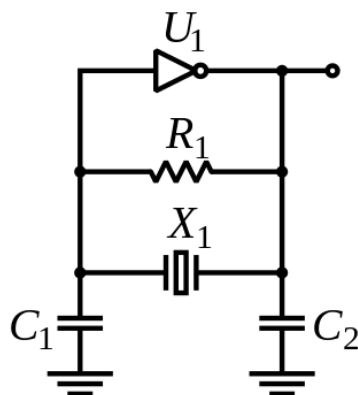


Figure 16. Pierce oscillator.

However, as the application of QCM has expanded to various sensing methods, the coating to improve QCM sensitivity is unavoidable, and unfortunately, those coatings are often viscous. This loading makes the traditional oscillator circuit unstable or inaccurate. The redesign of oscillator circuits needs to be considered.

The Miller oscillator is another circuit that gained the interest of many researchers since it is better in terms of maintaining the loop gain and phase for the oscillation in a wide margin of loss resistances, which is unavoidable in viscous film or liquid media. The design parameters optimization was proposed by Rodríguez-Pardo et al. [53] and was applied to the miller oscillator in liquid [54]. The circuit of their design worked with 10% glycerol accompanied with the low Q-factor down to 2586.

The renowned commercial QCM200 system is based on an Automatic Gain Control (AGC) oscillator [55]. Figure 17 shows the system's oscillating circuit design. The uncompensated QCM sensor is connected to the positive branch of a center-tapped transformer, while for the negative branch there is a variable capacitor compensating for C_v by adjusting

the C_v value that resulted in the canceled out the current between C_0 and C_v . This total compensation is identified as the point of maximum conductance when the frequency of the RF voltage source is swept. Many researchers have applied this system to various applications, such as biosensors [56] and humidity sensors [57].

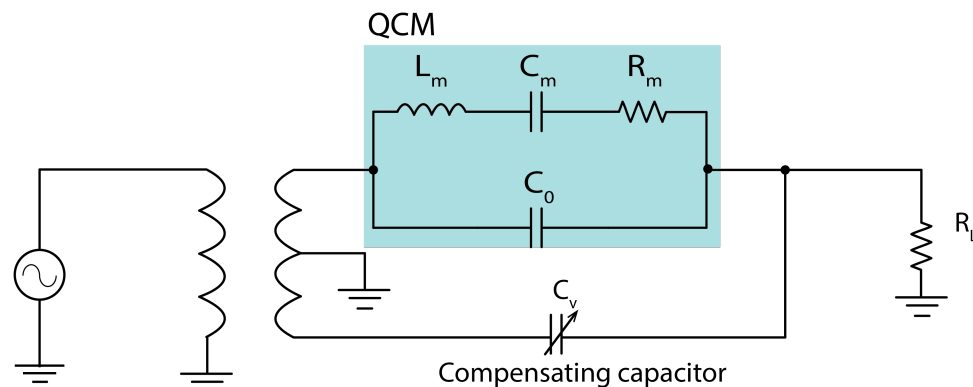


Figure 17. QCM oscillator with parallel capacitance compensation.

An emitter-coupled oscillator is another configuration of an oscillator, in which the design consists of two-state common emitter transistors [58]. With two inverted amplification states, it covers the loop-phase requirement and forces the crystal to operate at its zero-phase point, which corresponds fairly well to the motional series resonance frequency for high Q crystals with uncompensated C_0 . However, the QCM zero-phase point is considerably deviated from motional series resonance frequency for highly-loaded crystals (low Q). The recently reported design replaced double transistors with an Operational Transconductance Amplifier (OTA). This improved gain and biasing stability. This improved design is adequate to work in a liquid environment [59].

A bridge oscillator is another in the focus of QCM electronic interfacing systems based on standard, active and lever bridge oscillators. The lever bridge loop gain increased with the motion resistance (R_m) of the QCM. The lever bridge was also successfully used in a liquid environment [60]. However, the lever bridge needs a fast response in the gain change of OTA due to loading condition change, or else the oscillation cannot be stably maintained. The active bridge design was recently optimized and can be used under high liquid loading [61].

5.2. Dedicated Circuits

The dedicated circuit enables us to use the motional admittance branch of the QCM directly related to the detected properties. There are several proposed techniques that mainly focus on extracting both series resonant frequency and Q -factor or series resistance.

The exponentially decayed technique maybe is the most prominent technique in determining both resonant frequency and dissipation, which provides enough information about the QCM. Using the oscillator circuit together with a relay switch to separate QCM from the oscillator circuit is shown in Figure 18. The oscillation signal decays over time and is inversely proportional to the dissipation factor. The performance of this system was tested by a droplet of aqueous glycerol solution [62]. This system was later adopted into the commercial Q-sense system and was very ubiquitous among biosensing applications. The system was also expanded by the same research group, with the improvement in the dual-frequency drive of the resonator at two different harmonic overtones [63].

The phased-locked technique aims to lock the oscillation frequency to that of the motional series resonance frequency, which directly represents the QCM behavior, making it easier to interpret the QCM response. There are two types of these techniques, zero-phase and maximum conductance. Both of them utilize the Phase Lock Loop (PLL) oscillator to feed the driving frequency to QCM.

The zero-phase oscillator circuit consists of the amplification state, the compensation to state cancel out the C_0 branch of the BVD circuit, and the current-to-voltage converter (I-V con.). Figure 19 shows the PLL circuit with manual C_0 compensation. This circuit requires the calibration to cancel out the current I_c and cancel out the I_p , leaving only I_m , which simplified the QCM BVD equivalent circuit to having only a motional admittance branch. The practical implementation was achieved by Hu et al. [64]. The drawback was the need to re-compensate for C_0 if the QCM was changed or due to temperature change affecting the C_0 value.

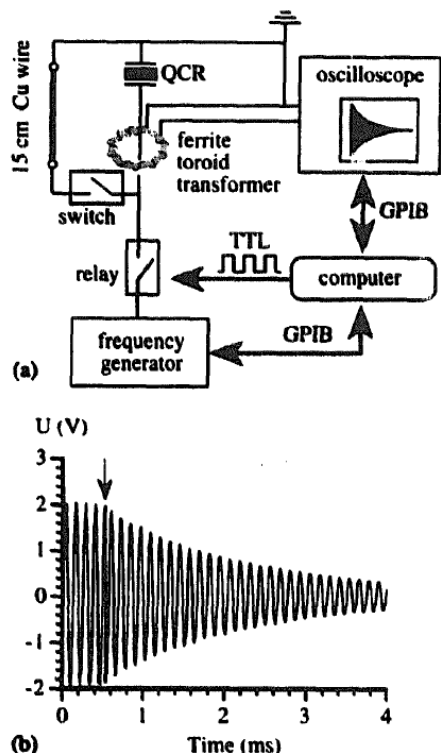


Figure 18. Circuit block diagram: (a) Schematic diagram. (b) Circuit diagram in detail. Reprinted from Sensors and Actuators B: Chemical, 37, Rodahl M. and Kasemo B., Frequency and dissipation-factor responses to localized liquid deposits on a QCM electrode, 111–116, (1996), with permission from Elsevier [62].

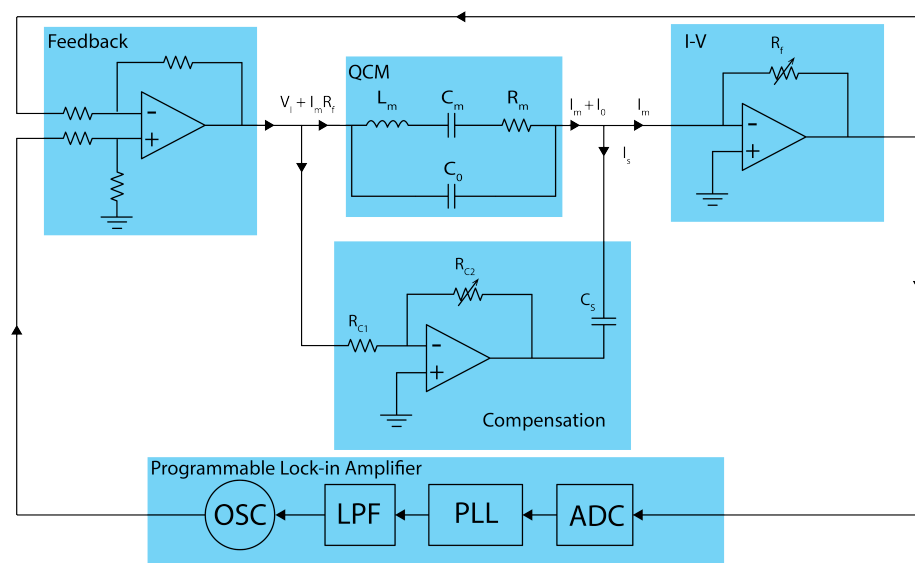


Figure 19. PLL circuit for series resonant tracking with manual C_0 compensation. Redrawn from [64] under the Creative Commons CC BY 4.0 license.

The maximum conductance oscillator circuit bypasses the C_0 compensation problem by tracking the maximum conductance instead. The maximum conductance represents only the motional admittance without involving C_0 . However, a current sensing component is needed to monitor the QCM current [65]. The current component is synchronous with the applied voltage and was extracted using the multiplier followed by a low pass filter, as is shown in Figure 20. The maximum conductance can be found when the frequency of VCO is swept.

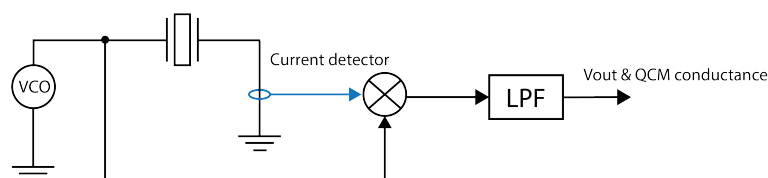


Figure 20. Circuit block diagram to obtain maximum conductance.

5.3. Vector Network Analyzer

One of the biggest advantages of VNWA is that the resonant frequency of QCM can be directly extracted from the measurement. The frequency of the oscillation cannot always agree with the resonant frequency change, and the oscillation frequency is smaller when the loss increases [66]. This effect is illustrated in Figure 21. Furthermore, the QCM sensor can be characterized without the influence of external circuitry. This method is considered to provide the most accurate measurement compared to any other technique. The loss due to viscous loading cannot be avoided, and we can overcome this problem by using VNWA.

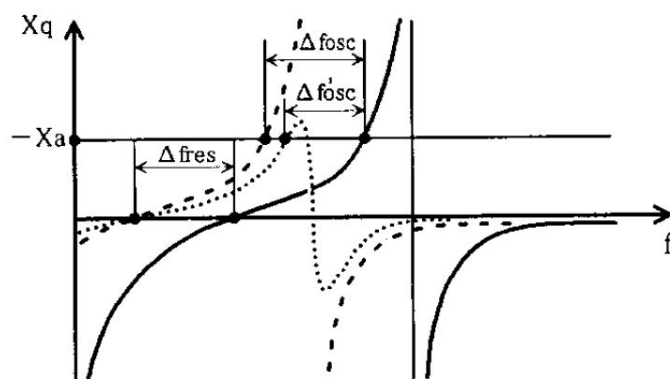


Figure 21. Dependency of reluctance upon frequency, solid line: no coating and no sorption. Thick dashed line: only mass loading without loss increase. Thin dash line: mass loading with additional loss. X_a is the circuit reactance at the oscillating point. Oscillation frequency deviates from actual resonant frequency change when loss increases. © 2021 IEEE. Reprinted with permission from 1996 Proceedings of the IEEE Ultrasonics Symposium, 1996, Volume 1, No. 22, pp. 351–354 [66].

The Vector Network Analyzer is used to characterize a two-port network such as an amplifier and a filter. The Vector Network Analyzer measures both the reflected signal from the input side and the signal passing through the Device Under Test (DUT) to its output side. The VNWA measurement is based on the S parameter. The S parameter represents the ratio of transmitted or reflected voltage to the incident voltage. The S_{11} parameter is commonly used for QCM measurement. It indicates the ratio of the reflected signal from port1 ($\frac{b_1}{a_1}$), where a_1 is incident voltage at port 1 and b_1 is reflected voltage at port 1. The basic diagram of the Vector Network Analyzer is as shown in Figure 22.

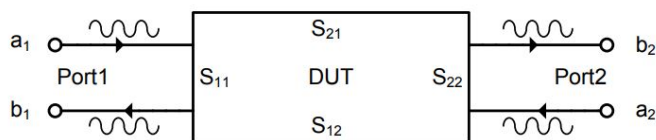


Figure 22. Basic concept of a Vector Network Analyzer.

To compensate for interface mismatch of the network analyzer and QCM, a PI network was proposed for QCM load matching [67]. However, the exact QCM parameter may not be necessary for sensor application.

Typical VNWAs are considerably large laboratory equipment and are not suitable for portable applications. The use of full-size VNWA was reported for pollen sensing [68]. The gas sensing applications also reported the use of VNWA to analyze the QCM response to NH_3 gas when the ZnO nanorod was synthesized on QCM. However, the dissipation factor was not utilized in data analysis [69]. To determine the improvement in sensitivity after modifying the QCM surface with Parylene-C, in Figure 23, the authors chose a peak-to-peak value of measured impedance to indicate the signal-to-noise ratio [70]. The peak-to-peak value was evaluated similarly to the Q factor, and it was found that after film deposition, the peak-to-peak value was slightly improved. The author interpreted that the increase in the peak-to-peak value might be caused by the piezoelectricity property of the Parylene-C layer, which reduced the energy dissipation of the QCM. The commercially available small-size VNWA with the function to measure dissipation was investigated and was compared with full-size VNWA. The results showed a difference of frequency measurement of 0.2%. This encouraged us to use small-size VNWA [71].

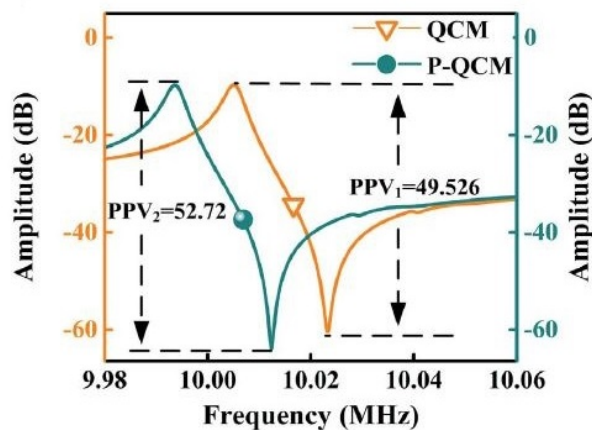


Figure 23. Evaluation of peak-to-peak value between typical QCM and Parylene-C coated QCM in air. Reprinted from *Biosensors and Bioelectronics*, 98, Yang et al., Stability enhanced, repeatability improved Parylene-C passivated on QCM sensor for aPTT measurement, 41–46, (2017), with permission from Elsevier [70].

We used the commercially available small-size VNWA. Its example is shown in Figure 24. This enables on-site measurement with an array of QCM sensors. Some researchers develop their own compact VNWA for QCM arrays utilizing a Direct Digital Frequency Synthesizer (DDFS) for frequency sweeping [72]. Another compact design VNWA was fabricated utilizing Programmable Logic Device (PLD) to control the operations. Similarly, DDFs were also used to produce sweep sinusoidal frequency. The sensor response is fed back to the network through the RMS to DC converter block (TRMS) back to PLD [73]. We recently used four VNWAs simultaneously to investigate the response of QCM sensors coated with Room Temperature Ionic Liquid (RITL) for odorant sensing [74].



Figure 24. Small-sized Vector Network Analyzer.

We also investigated the SNR improvement of the QCM measurement with VNWA [75], and the optimized sweeping parameters together with the curve-fitting technique followed by the Savitzky–Golay digital filter. Figure 25A shows the curve-fitting result to obtain circuit components, and Figure 25B shows the reduced signal fluctuation compared with the motional admittance method (see Figure 10). The measurement system was evaluated using a highly viscous glycerol solution (40% *w/w*). The summary of the QCM measurement methods is shown in Table 3.

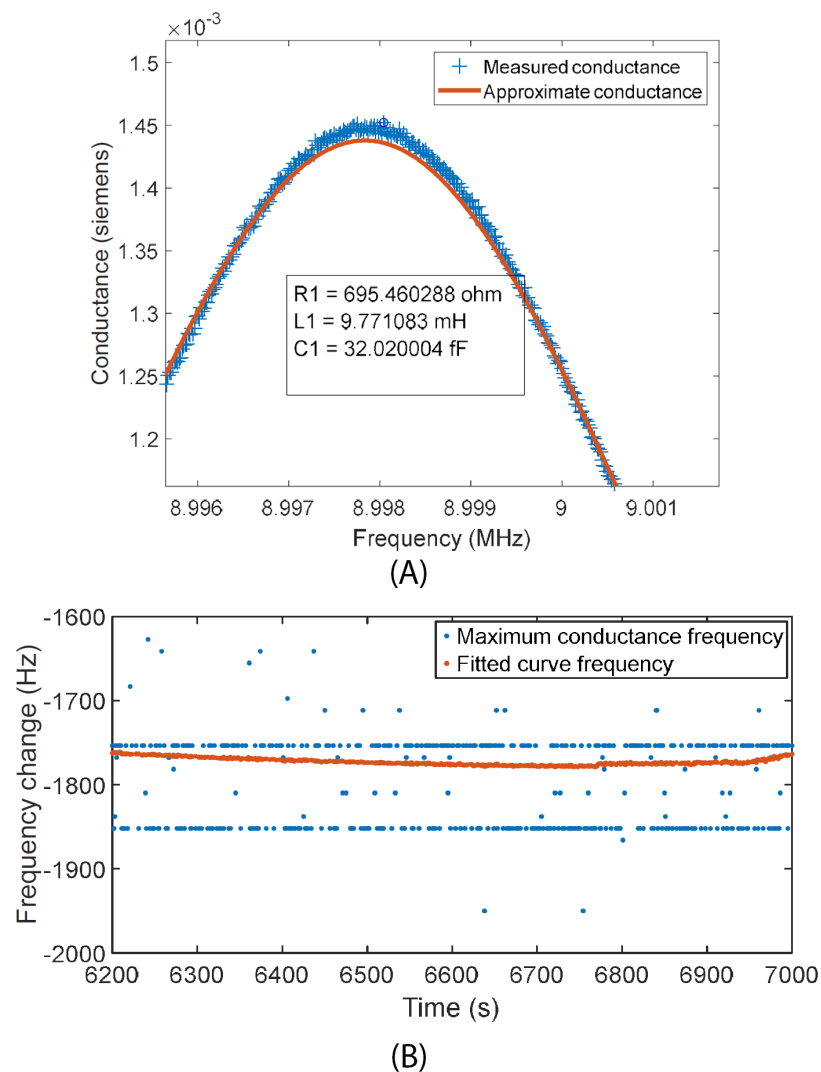


Figure 25. Improvement of signal-to-noise ratio for the VNWA measurement. **(A)** Curve fitting using the equivalent circuit. **(B)** Comparison of data obtained by curve fitting and raw maximum conductance measurement. © 2021 IEEE. Reprinted, with permission, from IEEE Sensors Journal, 2019, Volume 19, no. 22, pp. 10386–10392 [75].

Table 3. Summary table of measurement methods.

Measurement Methods	Advantages	Disadvantages
Oscillator circuit	Simple circuit design, only frequency counter is needed to measure oscillation frequency.	At high viscous loading, the circuit cannot maintain its positive feed back to continue oscillating.
Dedicated circuit	Additional parameter, i.e., resistance change, can be measured. Not the oscillation frequency but the resonant frequency is obtained.	Complicated design, need special knowledge to debug and fine-tune the system.
Vector Network Analyzer	Commercially available, sampling time and sweep frequency are adjustable.	Motional admittance method is not robust at highly viscous loading. Data curve fitting technique of the conductance curve help aids this drawback.

6. Experiment on QCM with Viscous Loading

As mentioned in Section 4.3, the thin viscous film can roughly represent the coating for the QCM sensor. The experiment on the viscous film when exposed to the analyte (water) was conducted. Figure 26 shows the simplified one-dimensional model of the film change when exposing it to water. The water sorption causes the overall film thickness to increase and the film viscosity to decrease. This assumption is expected to be able to adequately explain the experimental data, which were conducted with glycerol and Polyethylene Glycol (PEG) with two different molecular weights as film materials [76].

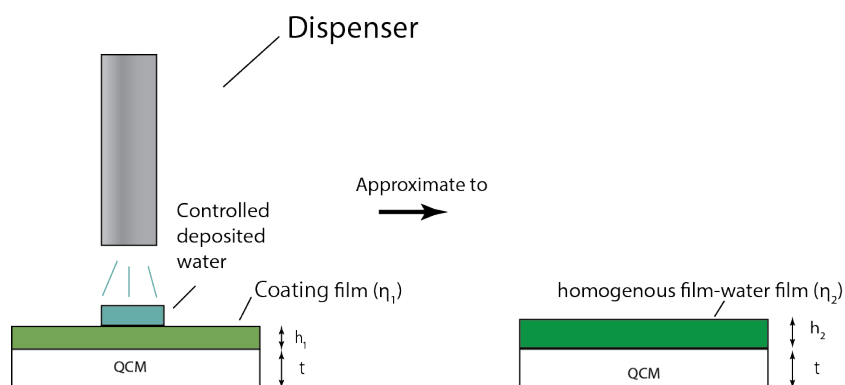


Figure 26. Simplified model of expected film change when exposed to water. Reprinted from [76] under the Creative Commons CC BY 4.0 license.

The three different materials were coated on the QCMs using the dip-coater. Then, the microdispenser was used to simulate the analyte exposure. Table 4 shows the QCM frequency and resistance change before and after coating. Glycerol had the highest frequency and resistance changes, indicating that glycerol is highly viscous.

Table 4. Film coating conditions.

Film Materials	f_{pre} (Hz)	f_{post} (Hz)	Δf (Hz)	R_{pre} (Hz)	R_{post} (Hz)	ΔR (Hz)
Glycerol	900,4436	8,991,551	−12886	19	740	721
PEG20M	900,1721	8,999,474	−2246	15.92	18.28	2.36
PEG2000	900,1739	8,999,439	−2300	10.98	172.22	161.2

Then, the QCMs coated with glycerol films were exposed to water in the order of 1 pulse, 3 pulses, 10 pulses, 30 pulses, and 100 pulses, respectively. For both PEG films,

the exposure was performed in the order of 100 pulses, 300 pulses, and 1000 pulses. The frequency and resistance shifts were plotted on the calculated contour plot of both frequency and resistance shift. Figure 27 shows the experimental result of water sorption with glycerol coating. The blue arrow line in Figure 27 shows the direction of the frequency drift, which in this case pointed toward the negative frequency shift. The orange arrow shows the peak frequency and resistance change after each deposition. The previous assumption that viscosity decreases as film thickness increases can roughly explain the data. Interestingly, although the negative frequency shift became larger, the resistance became almost constant. This can be explained in the case of 100 pulses. The change might occur along the resistance contour line, but the frequency change still occurs in effect. This can explain why sometimes a frequency change occurs without a resistance change.

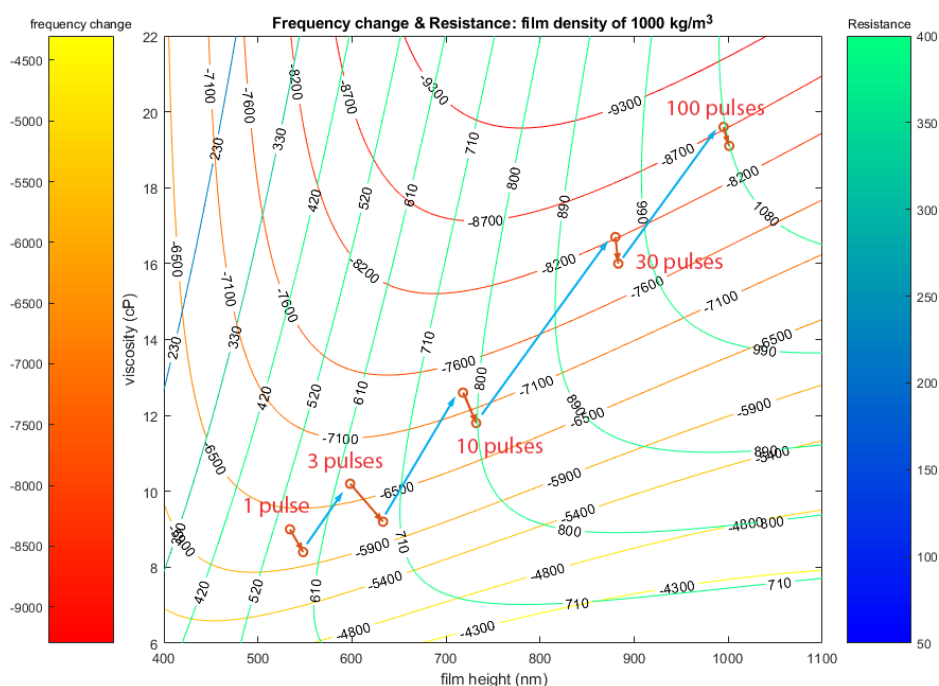


Figure 27. Combined contour plot of both resistance and frequency when glycerol film is exposed to water. The orange represents the frequency and resistance change of the coated QCM when exposed to water; the blue arrow indicates the direction of the frequency drift. Reprinted from [76] under the Creative Commons CC BY 4.0 license.

Similarly, Figure 28 shows the combined contour plot of both the frequency shift and resistance. The frequency shift and resistance data at 100 pulses are drawn for the PEG20M film and the PEG2000 film. PEG20M shows the tendency of frequency decrease while resistance increases. On the contrary, PEG2000 shows the tendency of frequency increase and resistance increase. The Mason equivalent circuit can explain the positive frequency change that occurs together with the positive resistance change. Figure 29 shows the raw data frequency change and resistance change of PEG2000 when exposed to water. The positive frequency change occurs on every deposition.

The data points that fall near the bottom right of the contour plot in Figure 28, show that the frequency change has a tendency toward positive change (increasing) due to the contour lines of the frequency change relatively parallel to the film height, making the positive frequency change occur when the viscosity decreases. On the contrary, data near the top left have an inverse effect: the frequency decreases when the film thickness increases. The resistance increased, for almost every case, when there was additional loading. This can be explained by the contour plot. The resistance contour lines always lie diagonally when the viscosity is over 1 cP (viscosity of water = 0.89 cP), which is always the case for almost every coating film. Interestingly, for the thin film (<50 nm), the film behaved as

a mass loading only, regardless of the viscosity. We can estimate the film thickness quite accurately by utilizing only the frequency change if the film thickness is thin enough.

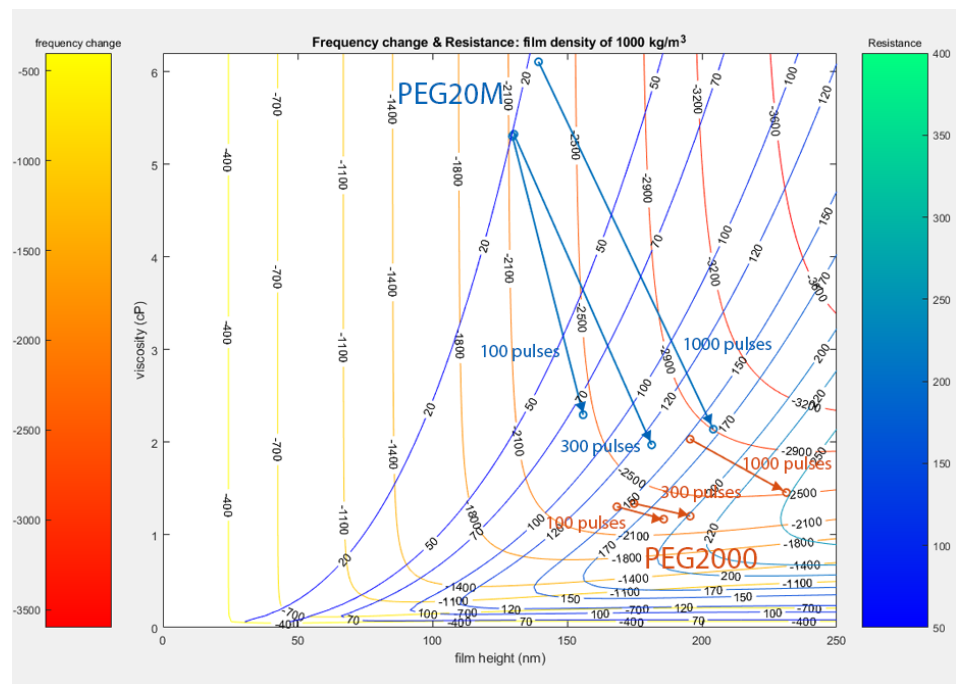


Figure 28. Combined contour plot of both resistance and frequency change when PEG films are exposed to water. The arrow line represents the frequency and resistance change of the coated QCM when exposed to 100, 300, and 1000 pulses of water; blue arrow: PEG20M, orange arrow: PEG2000. Reprinted from [76] under the Creative Commons CC BY 4.0 license.

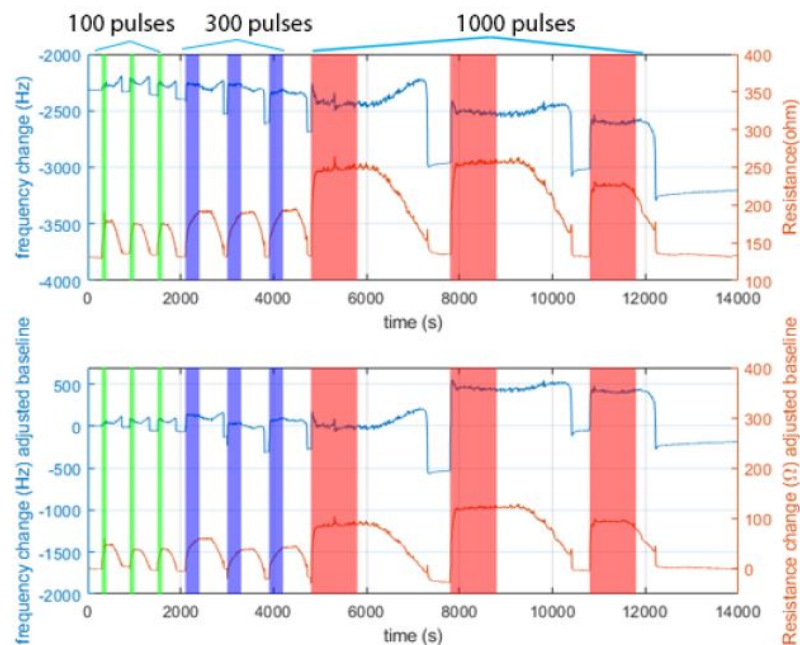


Figure 29. Response of QCM coated with PEG2000 when exposed to water. The color bar means period of exposure. Blue line: frequency shift. Orange line: resistance change. Top figure shows the raw data, and bottom figure shows the data after adjusting baseline before each deposition. Reprinted from [76] under the Creative Commons CC BY 4.0 license.

7. QCM Behavior Characterization

The behavior of QCM when exposed to non-conventional loading has not been thoroughly studied yet since we do not have any effective method to model every type of QCM response. One can make a regression model using machine learning. However, it is still important to develop a model that can represent the QCM response based on acoustic wave theory since it may help in understanding the underlying physics when the analyte binds with the sensing film.

QCM behavior modeling is being continuously developed. The sensitivity to film coating and the complexity of bonding to these layers makes the detection behavior more complicated. In this section, we will discuss the proposed models from various researchers.

There was a proposal of the ‘missing mass’ concept, which modified the mass term in the Sauerbrey equation, making the equation also applicable to viscous film loading [77]. The effect of ‘missing mass’ predicts the reduction of surface masses M_s in liquid phase measurements compared with the ‘true’ mass M of the film:

$$M_s = M \left\{ 1 - \frac{\eta_2 \rho_2 \omega}{\rho_1} \frac{G''}{G'^2 + G''^2} \right\}, M = \rho_1 h_1 \tag{30}$$

Some researchers proposed the sensitivity of QCM sensor in terms of phase shift [78]. This equation showed that the phase shift depends on the ratio of coating mass over the summation of an unperturbed resonator and the liquid.

$$\phi \cong -\Delta m_c / (m_q + m_L), \Delta m_q = \eta_q \pi / 2 v_q, m_L = \rho_L \delta_L / 2 \tag{31}$$

To differentiate the QCM response between mass loading and viscous loading is the challenge of using a QCM sensor in a liquid environment [79]. Since the usage of VNWA has become more popular, the QCM conductance measurement showed that the frequency at the half maximum point does not shift, as shown in Figure 30, where f_h is the frequency at half maximum conductance and f_p is the frequency at the maximum conductance.

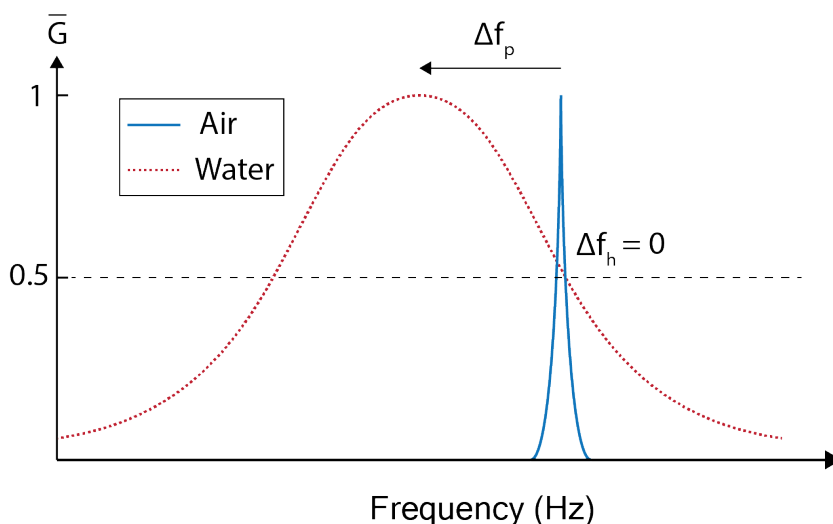


Figure 30. The simulation of normalized conductance curve of QCM in contact with air and water. The frequency at half maximum point does not change under viscous loading.

The separation between the viscosity and density of the liquid is also one of the most challenging problems for using QCM in a liquid environment. Typically the frequency change is proportional to $\sqrt{\rho_L \eta_L}$, where ρ_L is the liquid density and η_L is the liquid viscosity. One study on this problem proposed that the frequency shift was not only expressed by $\sqrt{\rho_L \eta_L}$ but also the overall liquid volume and density in equation

$$\Delta f = K_{pf} \Delta P f_0 + K_{Tf} \Delta T f_0, \tag{32}$$

where K_{pf} is the pressure–frequency sensitivity coefficient, K_{Tf} is the stress–frequency sensitivity coefficient, ΔP is the pressure variation, and ΔT is the stress variation. The stress change caused by the liquid properties is:

$$\Delta T = C_{Lf} \sqrt{\rho_L \eta_L} \quad (33)$$

The pressure change induced by the added liquid on the upper surface of the QCM sensor can be given as:

$$\Delta P = \rho_L C_{pf} V_L \quad (34)$$

where C_{pf} is the pressure frequency coefficient, and V_L is the liquid volume loaded onto the sensor surface. Using these two equations, they could obtain viscosity and density when at least two various liquid volumes were measured [80].

Since the QCM has become more popular in biosensing applications, recent research of the QCM model focusing on the living cells' immobilization was developed [81]. This model focused on spherical particle attachment in a liquid environment. The result was the modification of the equivalent circuit.

There is also a developed model trying to explain positive frequency with a different concept. The authors proposed a QCM as two weights connected with two springs [82]. The simulation showed that under certain conditions, QCM may exhibit a positive frequency shift.

8. Conclusions

In this review paper, we explained the fundamentals of QCM sensors, the piezoelectric effect, its physical structure, and the working principle. We surveyed several recent QCM sensor applications. Then, we described the theory of QCM behavior based on the Mason equivalent circuit and also showed the parameters of the equivalent circuit. We showed the QCM response of a conventional rigid thin film, bulk liquid and viscous film, including both simulation and experiment results. Then, we explored the measurement methods of QCM sensing. Lastly, we reviewed various mathematical models, which many researchers propose to explain the more complicated response of QCM sensors when they are coated with more complicated sensing film structures.

The conventional Sauerbrey's and Kanazawa's equations have limitations under the conditions of thin film and bulk liquid. The Mason equivalent circuit helps us predict a further generalized response of QCM coated with rigid film, viscous film, and expanding to bulk liquid, depending on the boundary conditions. The Mason equivalent circuit model provided us with a simplified explanation of the positive frequency change during sorption. The benefit of using Mason's equivalent circuit comes from the fact that an analytical solution was obtained. This provided us with an explanation of the phenomenon when the film parameters change. This expands our understanding of the relationship between film thickness and frequency change.

Lastly, the study of QCM behavior not only helps us understand its behavior but also may help us optimize the parameters for a better sensitivity, as some portion from the viscosity and film thickness contour plot has a high slope region. Furthermore, the investigation to explain the behavior of positive frequency change can be further improved by considering the film density or adopting the concept of complex viscosity. The latter case may improve the understanding of QCM behavior since the concept of energy storage and dissipation are included in the model.

Author Contributions: Conceptualization, T.N.; methodology, T.N. and S.N.S.; software, S.N.S.; validation, S.N.S.; formal analysis, S.N.S.; investigation, S.N.S.; resources, T.N.; data curation, S.N.S.; writing—original draft preparation, S.N.S.; writing—review and editing, T.N.; visualization, S.N.S.; supervision, T.N.; project administration, T.N. All authors have read and agreed to the published version of the manuscript.

Funding: This research received no external funding.

Institutional Review Board Statement: Not applicable.

Informed Consent Statement: Not applicable.

Conflicts of Interest: The authors declare no conflict of interest.

Abbreviations

The following abbreviations are used in this manuscript:

QCM	Quartz Crystal Microbalance
PEG	Polyethylene Glycol
VNWA	Vector Network Analyzer

References

1. Oltra, R.; Efimov, I.O. Local sensitivity of an electrochemical quartz crystal microbalance: Spatial localization of the low frequency mode. *Rev. Sci. Instrum.* **1995**, *66*, 1136–1141. [[CrossRef](#)]
2. Avramov, I.D. A 0-phase circuit for QCM-based measurements in highly viscous liquid environments. *IEEE Sens. J.* **2005**, *5*, 425–432. [[CrossRef](#)]
3. Borngräber, R.; Schröder, J.; Lucklum, R.; Hauptmann, P. Is an oscillator-based measurement adequate in a liquid environment? *IEEE Trans. Ultrason. Ferroelectr. Freq. Control* **2002**, *49*, 1254–1259. [[CrossRef](#)] [[PubMed](#)]
4. Nakamoto, T.; Kobayashi, T. Development of Circuit for Measuring Both Q Variation and Resonant Frequency Shift of Quartz Crystal Microbalance. *IEEE Trans. Ultrason. Ferroelectr. Freq. Control* **1994**, *41*, 806–811. [[CrossRef](#)] [[PubMed](#)]
5. Sauerbrey, G. Verwendung von Schwingquarzen zur Wägung dünner Schichten und zur Mikrowägung. *Z. Phys.* **1959**, *155*, 206–222. [[CrossRef](#)]
6. Thompson, M.; Arthur, C.L.; Dhaliwal, G.K. Liquid-Phase Piezoelectric and Acoustic Transmission Studies of Interfacial Immunochemistry. *Anal. Chem.* **1986**, *58*, 1206–1209. [[CrossRef](#)]
7. Dybwad, G.L. A sensitive new method for the determination of adhesive bonding between a particle and a substrate. *J. Appl. Phys.* **1985**, *58*, 2789–2790. [[CrossRef](#)]
8. Hayden, O.; Lieberzeit, P.A.; Blaas, D.; Dickert, F.L. Artificial antibodies for bioanalyte detection—Sensing viruses and proteins. *Adv. Funct. Mater.* **2006**, *16*, 1269–1278. [[CrossRef](#)]
9. Latif, U.; Can, S.; Hayden, O.; Grillberger, P.; Dickert, F.L. Sauerbrey and anti-Sauerbrey behavioral studies in QCM sensors—Detection of bioanalytes. *Sens. Actuators B Chem.* **2013**, *176*, 825–830. [[CrossRef](#)]
10. Noi, K.; Iwata, A.; Kato, F.; Ogi, H. Ultrahigh-frequency, wireless mems qcm biosensor for direct, label-free detection of biomarkers in a large amount of contaminants. *Anal. Chem.* **2019**, *91*, 9398–9402. [[CrossRef](#)]
11. Kirkendall, C.R.; Kwon, J.W. Sub-picogram resolution mass sensing in a liquid environment using low-loss quartz crystal microbalance. In Proceedings of the IEEE Sensors, Waikoloa, HI, USA, 1–4 November 2010. [[CrossRef](#)]
12. Huang, G.S.; Wang, M.T.; Su, C.W.; Chen, Y.S.; Hong, M.Y. Picogram detection of metal ions by melanin-sensitized piezoelectric sensor. *Biosens. Bioelectron.* **2007**, *23*, 319–325. [[CrossRef](#)] [[PubMed](#)]
13. Shockley, W.; Curran, D.R.; Koneval, D.J. Trapped-Energy Modes in Quartz Filter Crystals. *J. Acoust. Soc. Am.* **1967**, *41*, 981–993. [[CrossRef](#)]
14. Speller, N.C.; Siraj, N.; Regmi, B.P.; Marzoughi, H.; Neal, C.; Warner, I.M. Rational design of QCM-D virtual sensor arrays based on film thickness, viscoelasticity, and harmonics for vapor discrimination. *Anal. Chem.* **2015**, *87*, 5156–5166. [[CrossRef](#)] [[PubMed](#)]
15. Speller, N.C.; Siraj, N.; McCarter, K.S.; Vaughan, S.; Warner, I.M. QCM virtual sensor array: Vapor identification and molecular weight approximation. *Sens. Actuators B Chem.* **2017**, *246*, 952–960. [[CrossRef](#)]
16. Addabbo, T.; Bertocci, F.; Fort, A.; Mugnaini, M.; Shahin, L.; Vignoli, V.; Rocchia, S. A DDS-based multi-harmonic frequency meter for QCM sensor applications. *Procedia Eng.* **2014**, *87*, 288–291. [[CrossRef](#)]
17. Pomorska, A.; Shchukin, D.; Hammond, R.; Cooper, M.A.; Grundmeier, G.; Johannsmann, D. Positive frequency shifts observed upon adsorbing micron-sized solid objects to a quartz crystal microbalance from the liquid phase. *Anal. Chem.* **2010**, *82*, 2237–2242. [[CrossRef](#)]
18. Ward, M.D.; Delawski, E.J. Radial Mass Sensitivity of the Quartz Crystal Microbalance in Liquid Media. *Anal. Chem.* **1991**, *63*, 886–890. [[CrossRef](#)]
19. Huang, X.; Bai, Q.; Hu, J.; Hou, D. A practical model of quartz crystal microbalance in actual applications. *Sensors* **2017**, *17*, 1785. [[CrossRef](#)]
20. Milioni, D.; Mateos-Gil, P.; Papadakis, G.; Tsortos, A.; Sarlidou, O.; Gizeli, E. Acoustic Methodology for Selecting Highly Dissipative Probes for Ultrasensitive DNA Detection. *Anal. Chem.* **2020**, *92*, 8186–8193. [[CrossRef](#)]
21. Kartal, F.; Çimen, D.; Bereli, N.; Denizli, A. Molecularly imprinted polymer based quartz crystal microbalance sensor for the clinical detection of insulin. *Mater. Sci. Eng. C* **2019**, *97*, 730–737. [[CrossRef](#)]
22. Farka, Z.; Kovář, D.; Skládal, P. Rapid detection of microorganisms based on active and passive modes of QCM. *Sensors* **2015**, *15*, 79–92. [[CrossRef](#)]

23. March, C.; García, J.V.; Sánchez, Á.; Arnau, A.; Jiménez, Y.; García, P.; Manclús, J.J.; Montoya, Á. High-frequency phase shift measurement greatly enhances the sensitivity of QCM immunosensors. *Biosens. Bioelectron.* **2015**, *65*, 1–8. [[CrossRef](#)]
24. Schumacher, R.; Borges, G.; Kanazawa, K.K. The quartz microbalance: A sensitive tool to probe surface reconstructions on gold electrodes in liquid. *Surf. Sci.* **1985**, *163*, L621–L626. [[CrossRef](#)]
25. Kitz, P.G.; Lacey, M.J.; Novák, P.; Berg, E.J. Operando EQCM-D with Simultaneous in Situ EIS: New Insights into Interphase Formation in Li Ion Batteries. *Anal. Chem.* **2019**, *91*, 2296–2303. [[CrossRef](#)] [[PubMed](#)]
26. Acharya, B.; Sidheswaran, M.A.; Yungk, R.; Krim, J. Quartz crystal microbalance apparatus for study of viscous liquids at high temperatures. *Rev. Sci. Instrum.* **2017**, *88*, 025112. [[CrossRef](#)]
27. Cao-Paz, A.M.; Rodríguez-Pardo, L.; Fariña, J.; Marcos-Acevedo, J. Resolution in QCM sensors for the viscosity and density of liquids: Application to lead acid batteries. *Sensors* **2012**, *12*, 10604–10620. [[CrossRef](#)] [[PubMed](#)]
28. Abudu, A.; Goual, L. Adsorption of crude oil on surfaces using quartz crystal microbalance with dissipation (QCM-D) under flow conditions. *Energy Fuels* **2009**, *23*, 1237–1248. [[CrossRef](#)]
29. Asai, N.; Shimizu, T.; Shingubara, S.; Ito, T. Fabrication of highly sensitive QCM sensor using AAO nanoholes and its application in biosensing. *Sens. Actuators B Chem.* **2018**, *276*, 534–539. [[CrossRef](#)]
30. Song, W.; Guo, X.; Sun, W.; Yin, W.; He, P.; Yang, X.; Zhang, X. Target-triggering multiple-cycle signal amplification strategy for ultrasensitive detection of DNA based on QCM and SPR. *Anal. Biochem.* **2018**, *553*, 57–61. [[CrossRef](#)]
31. Li, Q.; Gu, Y.; Jia, J. Classification of multiple chinese liquors by means of a QCM-based e-nose and MDS-SVM classifier. *Sensors* **2017**, *17*, 272. [[CrossRef](#)]
32. Capuano, R.; Martinelli, E.; Ghezzi, S.; Paolesse, R.; Di Natale, C.; D'Amico, A.; Santonico, M.; Pennazza, G. An investigation about the origin of the lung cancer signalling VOCs in breath. In Proceedings of the IEEE Sensors, Valencia, Spain, 2–5 November 2014; Volume 2014.
33. Saraoglu, H.M.; Selvi, A.O.; Ebeoglu, M.A.; Tasaltin, C. Electronic nose system based on quartz crystal microbalance sensor for blood glucose and hba1c levels from exhaled breath odor. *IEEE Sens. J.* **2013**, *13*, 4229–4235. [[CrossRef](#)]
34. Khadka, R.; Aydemir, N.; Carraher, C.; Hamiaux, C.; Colbert, D.; Cheema, J.; Malmström, J.; Kralicek, A.; Travas-Sejdic, J. An ultrasensitive electrochemical impedance-based biosensor using insect odorant receptors to detect odorants. *Biosens. Bioelectron.* **2019**, *126*, 207–213. [[CrossRef](#)] [[PubMed](#)]
35. Huellemeier, H.A.; Eren, N.M.; Ortega-Anaya, J.; Jimenez-Flores, R.; Heldman, D.R. Application of quartz crystal microbalance with dissipation (QCM-D) to study low-temperature adsorption and fouling of milk fractions on stainless steel. *Chem. Eng. Sci.* **2022**, *247*, 117004. [[CrossRef](#)]
36. Tang, Y.; Tang, D.; Zhang, J.; Tang, D. Novel quartz crystal microbalance immunodetection of aflatoxin B1 coupling cargo-encapsulated liposome with indicator-triggered displacement assay. *Anal. Chim. Acta* **2018**, *1031*, 161–168. [[CrossRef](#)]
37. Jayawardena, S.; Siriwardena, H.D.; Rajapakse, R.M.; Kubono, A.; Shimomura, M. Fabrication of a quartz crystal microbalance sensor based on graphene oxide/TiO₂ composite for the detection of chemical vapors at room temperature. *Appl. Surf. Sci.* **2019**, *493*, 250–260. [[CrossRef](#)]
38. Liu, L.; Fei, T.; Guan, X.; Zhao, H.; Zhang, T. Highly sensitive and chemically stable NH₃ sensors based on an organic acid-sensitized cross-linked hydrogel for exhaled breath analysis. *Biosens. Bioelectron.* **2021**, *191*, 113459. [[CrossRef](#)]
39. Zhang, D.; Chen, H.; Li, P.; Wang, D.; Yang, Z. Humidity Sensing Properties of Metal Organic Framework-Derived Hollow Ball-Like TiO₂ Coated QCM Sensor. *IEEE Sens. J.* **2019**, *19*, 2909–2915. [[CrossRef](#)]
40. Matsumoto, K.; Tiu, B.D.B.; Kawamura, A.; Advincula, R.C.; Miyata, T. QCM sensing of bisphenol A using molecularly imprinted hydrogel/conducting polymer matrix. *Polym. J.* **2016**, *48*, 525–532. [[CrossRef](#)]
41. Nakamoto, T.; Moriizumi, T. A theory of a quartz crystal microbalance based upon a mason equivalent circuit. *Jpn. J. Appl. Phys.* **1990**, *29*, 963. [[CrossRef](#)]
42. Mason, W.P. *Electromechanical Transducers and Wave Filters*; Van Nostrand: New York, NY, USA, 1942; p. 399.
43. Granstaff, V.E.; Martin, S.J. Characterization of a thickness-shear mode quartz resonator with multiple nonpiezoelectric layers. *J. Appl. Phys.* **1994**, *75*, 1319–1329. [[CrossRef](#)]
44. Lucklum, R.; Hauptmann, P. Δf - ΔR QCM technique: An approach to an advanced sensor signal interpretation. *Electrochim. Acta* **2000**, *45*. [[CrossRef](#)]
45. Nakamoto, T.; Suzuki, Y.; Moriizumi, T. Study of VHF-band QCM gas sensor. *Sens. Actuators B Chem.* **2002**, *84*, 98–105. [[CrossRef](#)]
46. Lu, C.S.; Lewis, O. Investigation of film-thickness determination by oscillating quartz resonators with large mass load. *J. Appl. Phys.* **1972**, *43*, 4385–4390. [[CrossRef](#)]
47. Hillier, A.C.; Ward, M.D. Scanning Electrochemical Mass Sensitivity Mapping of the Quartz Crystal Microbalance in Liquid Media. *Anal. Chem.* **1992**, *64*, 2539–2554. [[CrossRef](#)]
48. Keiji Kanazawa, K.; Gordon, J.G. The oscillation frequency of a quartz resonator in contact with liquid. *Anal. Chim. Acta* **1985**, *175*, 99–105. [[CrossRef](#)]
49. Cady, W.G. The piezo-electric resonator. *Proc. Inst. Radio Eng.* **1922**, *10*, 83–114. [[CrossRef](#)]
50. Barnes, C. Development of quartz crystal oscillators for under-liquid sensing. *Sens. Actuators A. Phys.* **1991**, *29*, 59–69. [[CrossRef](#)]
51. Satoh, T.; Ruslan, R.I.; Gotoh, S.; Akitsu, T. Double-resonance quartz crystal oscillator and excitation of a resonator immersed in liquid media. *IEEE Trans. Ultrason. Ferroelectr. Freq. Control* **2011**, *58*, 788–797. [[CrossRef](#)]

52. Binti Ruslan, R.I.; Satoh, T.; Akitsu, T. Voltage-controlled double-resonance quartz oscillator using variable-capacitance diode. *IEEE Trans. Ultrason. Ferroelectr. Freq. Control* **2012**, *59*, 738–745. [[CrossRef](#)]
53. Rodríguez-Pardo, L.; Fariña, J.; Gabrielli, C.; Perrot, H.; Brendel, R. Design considerations of miller oscillators for high-sensitivity QCM sensors in damping media. *IEEE Trans. Ultrason. Ferroelectr. Freq. Control* **2007**, *54*, 1965–1976. [[CrossRef](#)]
54. Rodríguez-Pardo, L.; Rodríguez, J.F.; Gabrielli, C.; Perrot, H.; Brendel, R. TSM-AW sensors based on Miller XCOs for microgravimetric measurements in liquid media. *IEEE Trans. Instrum. Meas.* **2008**, *57*, 2309–2319. [[CrossRef](#)]
55. Stanford Research Systems. *QCM200 Digital Controller: Operation and Service Manual*; Stanford Research Systems, Inc.: Sunnyvale, CA, USA, 2018.
56. Liu, N.; Han, J.; Liu, Z.; Qu, L.; Gao, Z. Rapid detection of endosulfan by a molecularly imprinted polymer microsphere modified quartz crystal microbalance. *Anal. Methods* **2013**, *5*, 4442–4447. [[CrossRef](#)]
57. Muckley, E.S.; Lynch, J.; Kumar, R.; Sumpter, B.; Ivanov, I.N. PEDOT:PSS/QCM-based multimodal humidity and pressure sensor. *Sens. Actuators B Chem.* **2016**, *236*, 91–98. [[CrossRef](#)]
58. Arnau, A. A review of interface electronic systems for AT-cut quartz crystal microbalance applications in liquids. *Sensors* **2008**, *8*, 370–411. [[CrossRef](#)]
59. Beißner, S.; Thies, J.W.; Bechthold, C.; Kuhn, P.; Thürmann, B.; Dübel, S.; Dietzel, A. Low-cost, in-liquid measuring system using a novel compact oscillation circuit and quartz-crystal microbalances (QCMs) as a versatile biosensor platform. *J. Sens. Sens. Syst.* **2017**, *6*, 341–350. [[CrossRef](#)]
60. Martin, S.J. Resonator/oscillator response to liquid loading. *Anal. Chem.* **1997**, *69*, 2050–2054. [[CrossRef](#)]
61. Rodríguez-Pardo, L.; Cao-Paz, A.M.; Fariña, J. Design and characterization of an active bridge oscillator as a QCM sensor for the measurement of liquid properties and mass films in damping media. *Sens. Actuators A Phys.* **2018**, *276*, 144–154. [[CrossRef](#)]
62. Rodahl, M.; Kasemo, B. Frequency and dissipation-factor responses to localized liquid deposits on a QCM electrode. *Sens. Actuators B Chem.* **1996**, *37*, 111–116. [[CrossRef](#)]
63. Edvardsson, M.; Rodahl, M.; Kasemo, B.; Höök, F. A dual-frequency QCM-D setup operating at elevated oscillation amplitudes. *Anal. Chem.* **2005**, *77*, 4918–4926. [[CrossRef](#)]
64. Hu, Z.; Hedley, J.; Keegan, N.; Spoor, J.; Gallacher, B.; McNeil, C. One-port electronic detection strategies for improving sensitivity in piezoelectric resonant sensor measurements. *Sensors* **2016**, *16*, 1781. [[CrossRef](#)] [[PubMed](#)]
65. Jakoby, B.; Art, G.; Bastemeijer, J. Novel analog readout electronics for microacoustic thickness shear-mode sensors. *IEEE Sens. J.* **2005**, *5*, 1106–1111. [[CrossRef](#)]
66. Nakamoto, T.; Nakamura, K.; Moriizumi, T. Study of oscillator-circuit behavior for QCM gas sensor. In Proceedings of the IEEE Ultrasonics Symposium, San Antonio, TX, USA, 3–6 November 1996; Volume 1. [[CrossRef](#)]
67. Liu, G.; Dong, Z.; Li, D.; Wang, Y. Impedance measurement of quartz crystal based on network analysis method. In Proceedings of the Fourth International Seminar on Modern Cutting and Measurement Engineering, Beijing, China, 10–12 December 2010; Volume 7997. [[CrossRef](#)]
68. Jenik, M.; Seifner, A.; Lieberzeit, P.; Dickert, F.L. Pollen-imprinted polyurethanes for QCM allergen sensors. *Anal. Bioanal. Chem.* **2009**, *394*, 523–528. [[CrossRef](#)] [[PubMed](#)]
69. Minh, V.A.; Tuan, L.A.; Huy, T.Q.; Hung, V.N.; Quy, N.V. Enhanced NH₃ gas sensing properties of a QCM sensor by increasing the length of vertically orientated ZnO nanorods. *Appl. Surf. Sci.* **2013**, *265*, 458–464. [[CrossRef](#)]
70. Yang, Y.; Zhang, W.; Guo, Z.; Zhang, Z.; Zhu, H.; Yan, R.; Zhou, L. Stability enhanced, repeatability improved Parylene-C passivated on QCM sensor for aPTT measurement. *Biosens. Bioelectron.* **2017**, *98*, 41–46. [[CrossRef](#)]
71. Zainuddin, A.A.; Nordin, A.N.; Rahim, R.A.; Ralib, A.A.M.; Khan, S.; Guines, C.; Chatras, M.; Pothier, A. Verification of quartz crystal microbalance array using vector network analyzer and openQCM. *Indones. J. Electr. Eng. Comput. Sci.* **2018**, *10*, 84–93. [[CrossRef](#)]
72. Mills, C.A.; Chai, K.T.; Milgrew, M.J.; Glidle, A.; Cooper, J.M.; Cumming, D.R. A multiplexed impedance analyzer for characterizing polymer-coated QCM sensor arrays. *IEEE Sens. J.* **2006**, *6*, 996–1002. [[CrossRef](#)]
73. Wudy, F.; Multerer, M.; Stock, C.; Schmeer, G.; Gores, H.J. Rapid impedance scanning QCM for electrochemical applications based on miniaturized hardware and high-performance curve fitting. *Electrochim. Acta* **2008**, *53*, 6568–6574. [[CrossRef](#)]
74. Alexandre, M.; Nakamoto, T. Study of room temperature ionic liquids as gas sensing materials in quartz crystal microbalances. *Sensors* **2020**, *20*, 4026. [[CrossRef](#)]
75. Songkhla, S.N.; Nakamoto, T. Signal Processing of Vector Network Analyzer Measurement for Quartz Crystal Microbalance with Viscous Damping. *IEEE Sens. J.* **2019**, *19*, 10386–10392. [[CrossRef](#)]
76. Songkhla, S.N.; Nakamoto, T. Interpretation of quartz crystal microbalance behavior with viscous film using a mason equivalent circuit. *Chemosensors* **2021**, *9*, 9. [[CrossRef](#)]
77. Voinova, M.V.; Jonson, M.; Kasemo, B. 'Missing mass' effect in biosensor's QCM applications. *Biosens. Bioelectron.* **2002**, *17*, 835–841. [[CrossRef](#)]
78. Arnau, A.; Montagut, Y.; García, J.V.; Jiménez, Y. A different point of view on the sensitivity of quartz crystal microbalance sensors. *Meas. Sci. Technol.* **2009**, *20*, 124004. [[CrossRef](#)]
79. Parlak, Z.; Biet, C.; Zauscher, S. Decoupling mass adsorption from fluid viscosity and density in quartz crystal microbalance measurements using normalized conductance modeling. *Meas. Sci. Technol.* **2013**, *24*, 085301. [[CrossRef](#)]

-
80. Tan, F.; Qiu, D.Y.; Guo, L.P.; Ye, P.; Zeng, H.; Jiang, J.; Tang, Y.; Zhang, Y.C. Separate density and viscosity measurements of unknown liquid using quartz crystal microbalance. *AIP Adv.* **2016**, *6*, 095313. [[CrossRef](#)]
 81. Tarnapolsky, A.; Freger, V. Modeling QCM-D Response to Deposition and Attachment of Microparticles and Living Cells. *Anal. Chem.* **2018**, *90*, 13960–13968. [[CrossRef](#)]
 82. Dultsev, F.N.; Kolosovsky, E.A. QCM model as a system of two elastically bound weights. *Sens. Actuators B Chem.* **2017**, *242*, 965–968. [[CrossRef](#)]